

4. TRANSFER STANDARD FILTER RADIOMETERS: APPLICATIONS TO FUNDAMENTAL SCALES

George P. Eppeldauer, Steven W. Brown, Keith R. Lykke

National Institute of Standards and Technology, Gaithersburg, Maryland, USA

4.1 Introduction

Traditionally, spectral radiant power responsivity measurements propagate the reference scale from radiant-power-measuring primary standard radiometers to instruments that make other types of radiometric and photometric measurements. Often, the most frequently measured radiometric quantities are irradiance and radiance, not optical power. Irradiance is used to describe the amount of radiant flux falling on a surface or reference plane. Radiance is the most commonly used radiometric quantity to characterize and measure extended sources such as lamps, screens, and blackbody radiators (see Chapter 1). Similarly, the most common photometric measurements are measurements of illuminance, the amount of optical radiation falling on a surface weighted by the response of the human eye, and luminance, the amount of radiation from a source weighted by the response of the human eye.

Transfer standard filter radiometers are used to maintain and propagate reference irradiance and radiance responsivity scales to other radiometric and photometric calibration facilities and to validate irradiance and radiance responsivity scales realized in different ways. In this chapter, we discuss the design, characterization, and calibration of transfer standard filter radiometers used to measure sources over the spectral range from the ultraviolet to the mid-infrared. In particular, we will discuss the use of filter radiometers in the visible spectral region for the validation and propagation of fundamental irradiance and radiance responsivity scales. In Section 4.2, we discuss basic principles involved in the design of filter radiometers. In Section 4.3, we describe design considerations of filter-based irradiance meters. In Section 4.4, radiance meters are discussed.

The construction of a reference standard radiometer depends not only on the type of radiometric application (e.g. radiance or irradiance measurements), but also on the calibration method developed for the instrument. The basic idea of modern radiometric measurements is to calibrate the responsivity of the transfer standard radiometer with the simplest possible

geometry against the highest-level radiometer standard and then to use the transfer standard radiometer for real applications. In Section 4.5, calibration and characterization issues are presented.

Use of filter radiometers reduces the number of steps in the calibration chain making it possible to significantly reduce the uncertainty in a variety of source measurements. Because of the shorter calibration chain, the calibration cost is reduced along with the measurement uncertainty in many source measurement applications. In Section 4.5, we describe applications of filter radiometers, including the derivation and maintenance of Systeme International (SI) units, the kelvin and the candela, from the reference spectral responsivity scales.

Detectors used in irradiance and radiance meters commonly have a broad spectral response; for example, silicon detectors respond to radiant flux from below 200 to beyond 1100 nm. Consequently, irradiance and radiance meters designed to measure sources with a broad spectral distribution are often equipped with optical filters for spectral selectivity. In these instruments, spectral characteristics such as the center wavelength and bandpass of the filters are important design issues that impact the overall performance of the instrument.

Filter radiometers are used in a wide variety of applications, for example to achieve the spectral selectivity necessary to provide information about a chemical process or to determine the temperature of a blackbody [1]. Filter radiometers are often designed to achieve a desired spectral response; luminance meters, illuminance meters, and colorimeters are filter radiometers with spectral responsivities designed to match target spectral distributions. Luminance and illuminance meters are designed to mimic the CIE photopic spectral luminous efficiency function, $V(\lambda)$, while colorimeters are multi-channel filter radiometers with individual channels designed to approximate the CIE color matching functions [2].

QA :1

In remote-sensing applications, filter radiometers are commonly used to monitor environmental parameters and physical processes. In these applications, filters are chosen based on their intended application. To monitor atmospheric processes, filters are often chosen to coincide with atmospheric absorption features [3] or to reject absorption features [4]. To monitor processes on land or in the oceans, filters are typically chosen to coincide with atmospheric transmittance windows to minimize effects of the intervening atmosphere on the measurement.

Another important field where irradiance meters play a large role is in the measurement of ultraviolet (UV) radiation [5]. A typical problem in this field is the measurement of the changes in the level of terrestrial solar UVB radiation to assess the effects of ozone depletion and its impact on biological systems. In this field, the measurement uncertainties of filter radiometers

with UV filters are high because of the instability and lower performance of the optical components (as compared to the visible range), such as sources, diffusers, filters, and detectors. Also, the intensity of natural UV radiation is low compared with the visible background. Because a meaningful global measurement program requires lower than 1% measurement uncertainties, careful design and calibration of these instruments is critical if they are to provide physically meaningful data.

Consideration of optical detector and filter elements is implicit in filter–detector-based optical metrology. Application-specific design issues—dependent on the radiometric quantity to be measured—primarily revolve around the geometrical constraints of the measurement. In radiant power responsivity measurements, the total power (radiant flux) leaving a source is measured by the detector. The unit of radiant power is the watt (W). The radiation to be measured has to under-fill the active area of the radiation-measuring detector. The geometrical design of power-measuring detectors and radiometers is simple. Usually, they do not need any input optics or defining apertures. An example is shown in Figure 4.1(a), where the total radiant power P in a laser beam is measured by a detector. Laser power

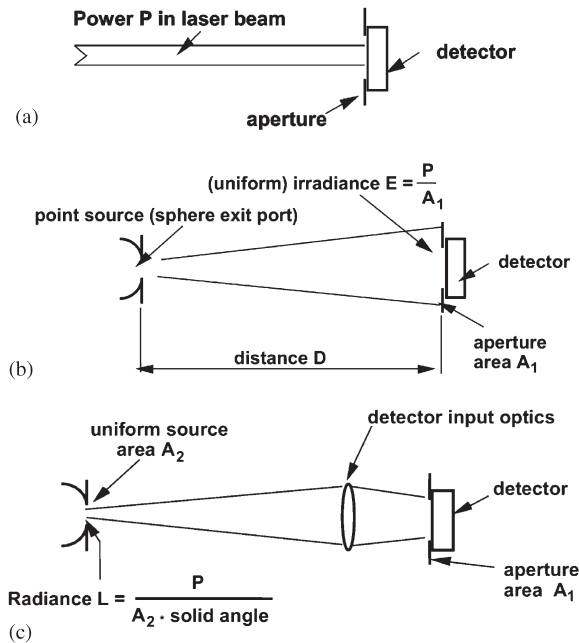


FIG. 4.1. (a) Simplified scheme of radiant power measurement. (b) Simplified scheme of irradiance measurements. (c) Simplified scheme of radiance measurements.

measurement is a practical example for detector radiant power responsivity measurement.

In irradiance measurements, the total radiant flux in a defined area in a reference plane is to be determined. The irradiance responsivity is the output current or voltage of the detector divided by the irradiance at the reference plane of the irradiance meter. A simplified scheme of irradiance measurements is shown in Figure 4.1(b). In the example shown, the meter's reference plane is the plane including the aperture with area A_1 . The radiant flux leaving the overfilled aperture (with a total radiant power P) must be entirely measured by the detector. In this case, the irradiance in the reference plane is equal to the measured power divided by the aperture area.

In radiance measurements, the radiant flux from a certain area within an extended source is measured. Figure 4.1(c) shows an example for the radiance (L) measurement of a sphere source. For comparison, the same detector and aperture with area A_1 can be used in the radiance meter as in Figure 4.1(b) for irradiance measurement. The difference between the two measurements is that the radiance meter is equipped with input optics (e.g. a lens) to image a spot from the source surface onto the detector. The target spot, subtended by the meter, must be located inside of the source aperture that has an area A_2 . The radiance measurement angle is determined by the input optics that includes the field stop aperture with area A_1 .

Calibrating a filter radiometer, designed for the measurement of the required radiometric quantity with the simplest possible geometry against the highest level radiometer standard, is one of the fundamental underlying principles of modern radiometric measurements. For radiant power, the detector responsivity is equal to its output current or voltage divided by the measured radiant power. The incident radiant power is determined from calibrations against a reference radiometer such as an electrical substitution cryogenic radiometer or silicon trap-detector. The irradiance responsivity scale is derived from the radiant power responsivity scale. In an ideal case, the irradiance responsivity of an irradiance meter is equal to the radiant power responsivity of its detector times the area of the detector aperture.

Radiance-measuring radiometers always need input optics that can image the radiant power from a target area of the source onto the detector. Note that the detector itself still measures optical power. In scale derivations, spatially uniform, Lambertian and extended sources (e.g. integrating spheres, see below) that overfill the radiometer entrance pupil are used as transfer calibration sources. The radiance responsivity of the meter is equal to the detector output current or voltage divided by the source radiance within the target area. Knowing the measurement geometry, the radiance of the transfer calibration source can be determined using an irradiance meter.

Using this method, the radiance responsivity scale is derived from the irradiance responsivity scale.

4.2 Common Design Considerations for Filter Radiometers

Selection of the appropriate detectors and filters for a given radiometric application is a critical step in the design of a filter radiometer to achieve low uncertainties in the propagation of reference spectral responsivity scales. A preamplifier, when it is used with a selected detector, should be designed to obtain low measurement uncertainty even at high signal gains. Also, the signal-to-noise ratio should be optimized for the output of the filter radiometer [6]. In many cases, detectors and filters have temperature dependences to their detector responsivity or filter transmittance. If the temperature sensitivity of the filter radiometer is significant in the designed wavelength range, temperature monitoring or control is needed. Typically, temperature control is simpler in practice than temperature monitoring which requires subsequent correction or temperature normalization to the data [7].

4.2.1 Detector Considerations

Spectral responsivity, spectral response linearity, long-term stability and temperature dependence are all important considerations in choosing the appropriate detector for the envisioned application. When radiant power responsivity scales are derived from a primary standard cryogenic radiometer, high spatial-response uniformity is needed as well. Of course, for scale realizations and propagations, the highest quality photodetectors are required to minimize the responsivity uncertainty of the device.

In the visible region, silicon detectors are most often used. For standard applications, Hamamatsu S1337 (or the equivalent S1336 or S6337) photodiodes are commonly used. A physical model of the internal quantum efficiency (IQE) has been developed for this type of photodiode and can be used for extrapolation and interpolation of its spectral responsivity [8]. The IQE is the ratio of the number of collected electrons to the number of photons absorbed by the detector after the front surface reflection loss. A device's external quantum efficiency (EQE) is defined as the IQE times $(1 - \text{reflectance})$. The reflection loss can be minimized in a device by arranging a number of photodiodes such that the reflection from one photodiode is incident on the next one in the "chain." In this configuration, the total device reflectance is equal to the reflectance from a single photodiode element to the n th power, where n is the number of photodiode elements in the device. A detector arranged in this type of configuration is known as a trap

detector. Because of their high IQE, connecting the S1337 detectors in parallel and measuring the sum of the photocurrents gives close-to-unity EQE. A trap detector built from S1337 photodiodes is frequently called a “quantum-flat detector” because of its extremely high EQE. The EQE of a tunnel-trap detector built from six S1337 photodiodes is a constant, 0.998, within 0.1%, between 500 and 900 nm. These photodetectors have exhibited excellent long-term radiometric stability and spatial response uniformity. A maximum-to-minimum change in the spectral power responsivity of less than 0.03% was measured on the NIST Spectral Comparator Facility (SCF) on four S1337 photodiodes from 1992 to 2002 between 405 and 920 nm. On average, the maximum-to-minimum variation in the spatial response of these 1×1 cm detectors was 0.3%.

The photodiodes of a trap detector should be specially selected for equal shunt resistance to keep the resultant shunt resistance reasonably high. High photodiode shunt resistance is needed in those applications where high sensitivity (small amplification for the amplifier input noise), low current-to-voltage conversion uncertainty, and excellent linearity are needed. In addition to excellent radiometric characteristics, the Hamamatsu S1227 (or S1226) silicon photodiodes have shunt resistances in the 1–10 G Ω range. These are more than an order of magnitude larger shunt resistances than that of the S1337. Compared with the S1337 photodiode, they have a suppressed responsivity in the near-infrared range and are frequently used for photometric and other visible applications. The noise-equivalent photocurrent that can be measured with a S1227 photodiode is 10^{-16} A [9].

Many applications require measurements in the UV and infrared (IR) regions, outside the spectral range appropriate for silicon detectors. Passivated detectors that are resistant to UV damage should be used for filter radiometers operating in the UV range. Such detectors are thick oxide nitrided Si (UVG-100), the thin oxide nitrided Si (AXUV-100G) photodiodes (commercially available from IRD) and platinum-silicide photodiodes [10]. Silicon photodiodes with platinum-silicide (Pt-Si) front windows have about a decade lower responsivity than the nitrided Si photodiodes.

In the IR range, germanium (Ge), indium gallium arsenide (InGaAs), and extended-InGaAs photodiodes are conveniently used in filter radiometers between 0.8 and 2.5 μm . Indium antimonide (InSb) detectors are used for the 1 to 5 μm spectral range and mercury cadmium telluride (MCT) detectors are used for the 2 to 26 μm spectral range.

IR detectors are often operated at reduced temperatures to reduce the background noise and improve their operational performance, for example, to increase their shunt resistance (discussed below). Cooling is especially important for Ge and InGaAs photodiodes because they have low shunt resistances at room temperature. As a result of cooling, the shunt resistance

can be increased significantly. As an example, the shunt resistance of a 5 mm diameter Ge photodiode increased from 17 k Ω at 25°C to 20 M Ω at -30°C. The shunt resistance change of a similar size InGaAs photodiode for the same temperature change was about 40 times smaller. However, the 25°C value was 2 M Ω [11]. Usually, a one-to four-stage thermoelectric (TE) cooler and a temperature-sensing thermistor are built into a photodiode can. The can is hermetically sealed with a window. The thermistor and the TE cooler thermal characteristics must be known to properly set the required (cold) constant temperature.

InSb detectors are typically placed in an evacuated dewar and operated at liquid-nitrogen temperatures (77 K). InSb detectors have an instability that occurs when short wavelength radiation is allowed to impinge on the detector. In this case, charges build up and are trapped in the device. Charge continues to build up until electric discharge occurs, resulting in a non-stable signal component, called InSb “flashing” [12], superimposed on the useful signal. Consequently, care should be taken when purchasing and using InSb detectors. The detector should have internal masking to minimize flashing and filtering to prevent short wave radiation from reaching the detector. Frequently, cold cut-on (high-pass) filters are used inside the dewar to block short wavelength radiation and minimize InSb flashing. The cut-on filter will set the low-end wavelength limit for the InSb filter radiometer. The upper cut-off wavelength of an InSb radiometer should be controlled by cold filters. An example for a 2.7 μm cut-off filter was shown in Chapter 3, Figure 3.5. An example for bandpass filter application will be shown later in this chapter (Figs. 4.21 and 4.22).

The maximum-to-minimum spatial response non-uniformity is within 1% even for large area (7 mm diameter) InSb detectors [13]. Less than 1% responsivity changes were obtained when the irradiance from blackbody radiators was measured over a time period of 1 year.

Detectors with known relative spectral responsivity are often used to extend the reference radiant power responsivity scale to the UV and IR ranges. Detectors with constant, flat responsivity versus wavelength are the most suitable devices for responsivity scale extensions. With the selection of high-quality pyroelectric detectors, pyroelectric radiometers can be developed for accurate responsivity scale transfer [14]. Using these pyroelectric radiometers, the sub-0.1% ($k = 1$) scale uncertainty in the silicon wavelength range will increase to 0.25% between 1 and 2 μm and the uncertainty will reach 0.34% at 2.5 μm [15]. In the UV spectral range between 125 and 320 nm, the relative combined standard uncertainty in the responsivity scale is less than 0.5% when UV damage-resistant detectors are calibrated against a cryogenic radiometer [16].

4.2.2 Filter Considerations

Filters are critical components of filter radiometers. Two types of filters are commonly used: colored glass filters and multilayer interference filters. Colored glass filters are used to block short- or long-wavelength radiation and to design instruments with a wide spectral bandpass, e.g. photometers and colorimeters. Interference filters are used in general when glass filters are not available or when a narrow spectral bandpass is required.

The color of filter glasses is determined by dissolving or suspending coloring agents in the glass. The optical density, or specific spectral transmittance of a filter, is controlled by the concentration of coloring agents in the glass or its thickness. Glass filters of different thicknesses that are cemented together are widely used in instruments such as in photometers and colorimeters.

A large variety of filters with different spectral transmittance curves can be realized with custom-made interference filters. The stability of interference filters has been a long-standing issue. To improve their radiometric performance, the high-reflectance multilayer coatings used in Fabry–Perot type filters can be sealed to protect the coatings from moisture. Also, the filters can be constructed from hard, durable, non-hygroscopic materials. In addition, the stability of interference filters has improved in the last several years with the development of ion-beam-assisted deposition (IBAD) of the dielectric layers that comprise the filter. IBAD filters are less sensitive to humidity, UV exposure, and temperature changes than conventional multilayer dielectric interference filters.

The transmission of interference-type filters depends on incident beam geometry. As the angle of beam incidence increases from the normal of the filter surface, the center wavelength shifts to shorter wavelengths. The lower the effective index of refraction, the greater the shift. Also, the filter transmittance is temperature dependent. It is important to keep the temperature coefficient of spectral transmittance low. The peak transmission wavelength increases and decreases with temperature in a linear fashion; nearly all optical filters exhibit a positive linear temperature coefficient.

Different types of filters have been used in the power and irradiance measuring radiometers discussed in this chapter. The out-of-band transmission of bandpass filters can range from 10^{-3} to 10^{-7} . Consideration of the out-of-band transmission is very important when filters are used with broadband sources and detectors. Flatness, parallelism, surface quality, and pinholes are important issues mostly for imaging applications. In order to keep measurement uncertainty low, high-performance interference filters are to be purchased and parallel beams and temperature control for the filter(s) should be applied.

Inter-reflections between the aperture and filters or between the filter and the detector can result in a responsivity that is dependent on measurement geometry. Inter-reflections between filter components is also a common problem. In order to avoid inter-filter reflections when more filters are used, the individual filters (filter layers) should be glued together using optical cement. In general, the lowest measurement uncertainty is obtained when the same beam geometry is used at both calibration and applications. The simplest solution is to use a “point-source” geometry.

4.2.3 Temperature Control

In many applications, both the photodiodes and the filters need temperature control to keep the responsivity change of the filter radiometer negligibly small when operated under different ambient temperatures. The temperature-dependent, radiant power responsivity changes of two silicon photodiodes frequently used in radiometers and photometers, Hamamatsu S1226 and S1337, are shown in Figure 4.2. At 700 nm (close to the long end of the visible range), the S1226 photodiode has a temperature coefficient of responsivity less than $0.05\%/^{\circ}\text{C}$. The temperature dependence increases nearly quadratically to longer wavelengths. At 1000 nm, the photodiode has a temperature dependence greater than $0.5\%/^{\circ}\text{C}$. A 4°C temperature difference between an instrument’s calibration and application will produce 0.2% responsivity change at 700 nm. In contrast, the Hamamatsu S1337 photodiode, widely used to propagate the spectral radiant power responsivity scale, has a negligible responsivity temperature coefficient below

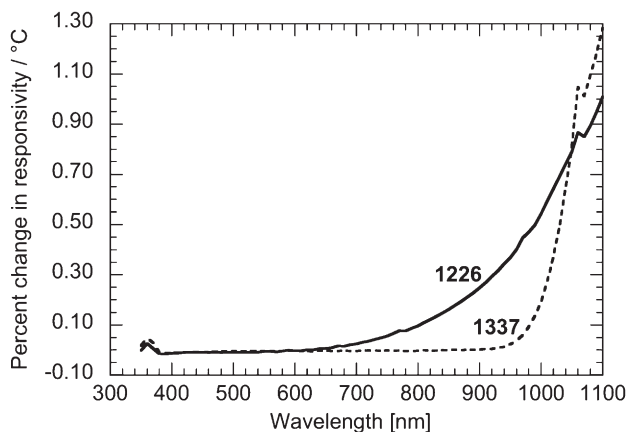


FIG. 4.2. The temperature coefficients of radiant power responsivity versus wavelength of Hamamatsu S1226 and S1337 silicon photodiodes.

940 nm. Instruments made from these photodiodes do not need temperature control up to this wavelength limit.

Filters can have a significant temperature dependence as well. For example, an illuminance meter measured the constant illuminance from a Standard Illuminant A source between 22°C and 29°C. A temperature coefficient of 0.083%/°C was obtained for the illuminance responsivity of the photometer. Figure 4.3 shows the linear curve fit to the measured data. The 0.083%/°C temperature coefficient was dominated by the temperature dependence of the cut-on edges of the individual filters used in the $V(\lambda)$ filter combination in front of the Hamamatsu S1226 silicon photodiode. The photodiode has a contribution to the temperature-dependent illuminance responsivity at wavelengths longer than 630 nm (see below).

Filters in radiometers are typically not cooled, but are maintained at a slightly elevated temperature using a separate temperature control loop. Temperature stabilization at a slightly elevated temperature rather than a lower temperature is typically used to avoid condensation on the filters. The filter radiometer illustrated in Figure 4.4 is a common design, where the temperature of the photodiode and the filter are controlled independently from each other.

Instruments using colored glass filters can be extremely stable if proper care is taken in the filter selection. For example, Figure 4.5 shows the measured relative stability of a group of standard illuminance meters over a 9-year period. The optical component packages in each illuminance meter contain a Hamamatsu S1226 silicon photodiode, a spectral filter, and an aperture in front of the filter. The filter between the aperture and the photodiode matches the spectral responsivity of the radiometer to the standardized CIE $V(\lambda)$ sensitivity of the human visual system [17]. The

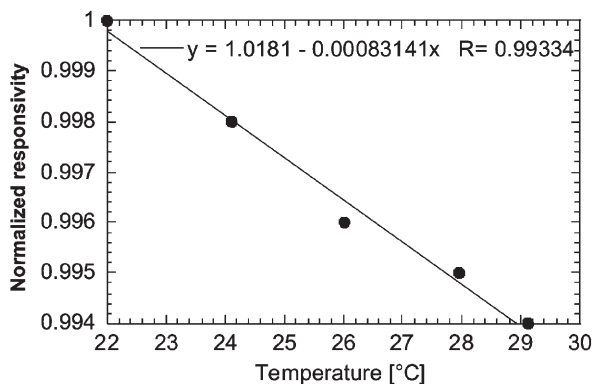


FIG. 4.3. Temperature-dependent responsivity of an illuminance meter.

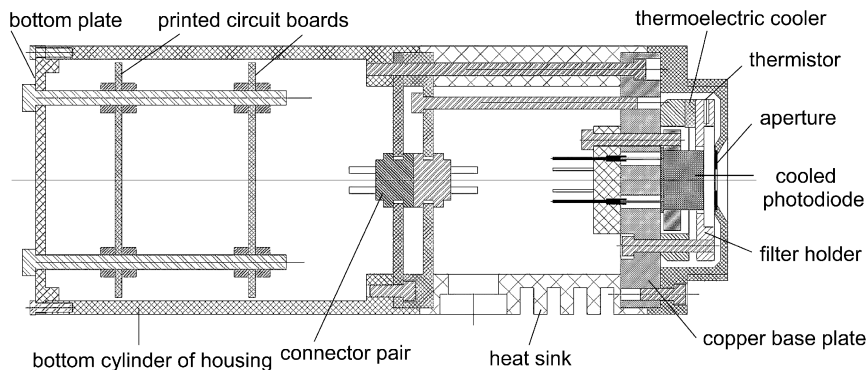


FIG. 4.4. Design of irradiance-meter head using single-element photodiode.

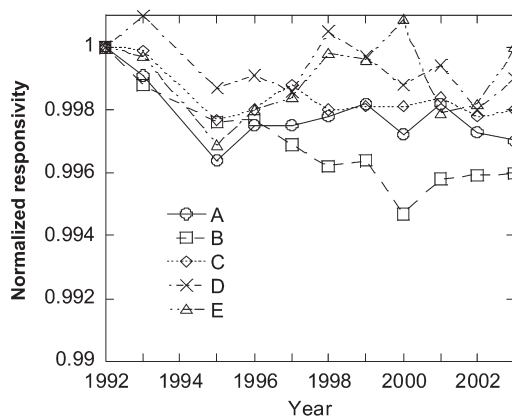


FIG. 4.5. Nine-year long stability of illuminance responsivity of a group of illuminance meters.

temperature of all filter-photodiode packages was monitored and corrections were applied for the illuminance responsivities as necessary.

The relative uncertainty of the yearly responsivity scale realizations was also 0.1%. Five illuminance meters were stable to within the repeatability of the measurements. Three instruments showed dramatic temporal changes in their relative responsivity. Each layer in the filter combinations used in the five stable radiometers shown in Figure 4.5 was an individually polished color glass filter [18]. Filter combinations for the three less stable illuminance meters were purchased from other commercial sources.

4.2.4 Preamplifier Design

The preamplifier is needed to measure the short-circuit current from the photodiode and to amplify the signal to obtain a high enough signal-to-noise ratio at the output. The preamplifier is the dominant amplification stage where the fundamental signal-to-noise ratio is determined. The preamplifier always measures the DC output of the photodetector. In general, the preamplifier characteristics must be matched to the impedance (shunt resistance and junction capacitance) of the detector if high measurement performance is to be achieved [6].

The simplest version of a widely used photocurrent meter is shown in Figure 4.6. The photocurrent of photodiode P is measured by a short-circuit current-meter. The current-to-voltage conversion in the current meter is realized by an operational amplifier (OA) and a feedback resistor (R) that has a parallel (stray) capacitance (C). This circuit diagram looks very simple. However, when low-uncertainty photocurrent measurements are needed over a wide dynamic signal range with a large signal-to-noise ratio in the output voltage V , the fundamental gains of the photocurrent meter need to be known. The fundamental gains are the signal gain, the loop gain, and the closed-loop voltage gain; each should be optimized for high accuracy measurements. The frequency dependent knowledge of the fundamental gains is especially important when the optical radiation is modulated. Signal chopping can be applied to tune the signal frequency outside of the $1/f$ noise range of low-frequency (DC) measurements. Also, in a measurement where the background signal component is large, such as in the infrared range, a modulated signal can be easily separated from the DC signal produced by the background radiation.

The equivalent circuit of the photocurrent meter of Figure 4.6 is shown in Figure 4.7. P has a shunt resistance R_S and a junction capacitance C_J which

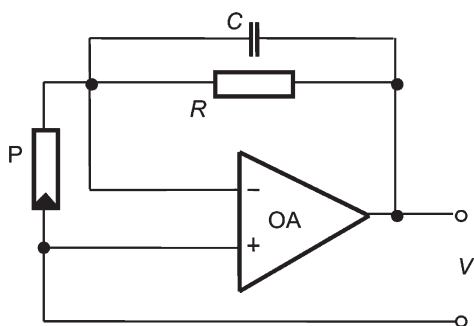


FIG. 4.6. Circuit diagram of a simple photocurrent meter.

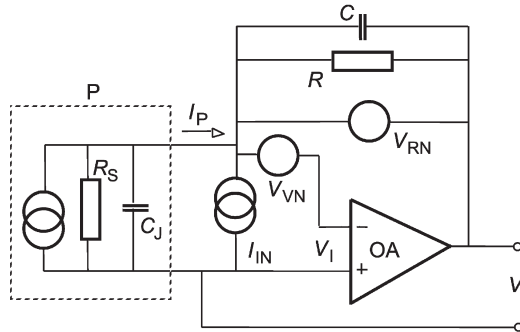


FIG. 4.7. Equivalent circuit of a photodiode short-circuit current meter.

together produce the photodiode impedance Z_d . The photocurrent I_P is converted into an output voltage V through the feedback impedance of the OA. The feedback impedance Z is the parallel connection of R and C . The OA input voltage V_I is the voltage between the inverting negative and non-inverting inputs. V_I is small because of the large OA open-loop gain, A . The open-loop gain is the ratio of the output voltage V to the input voltage V_I .

As the maximum of V is 10 V, and A is about 10^6 , V_I is equal to or smaller than $10\ \mu\text{V}$. This very small voltage drop on P produces a small load resistance (input resistance of the current meter) R_I for the photodiode [19]:

$$R_I = \frac{R}{A} \quad (4.1)$$

In case of low signal frequencies (DC photocurrent measurements), the requirement for linear short-circuit current measurements is $R_I \ll R_S$. Only low-frequency (DC) design considerations that can be applied for filter radiometers using silicon, UV, or near-to-mid-IR photodiodes are discussed in this chapter. The feedback impedance Z and the impedance of the photodiode Z_d create a feedback network from the OA output to the OA input. The voltage attenuation of the feedback network is β . Consequently, the characteristics of the three primary components in the analog control loop, the photodiode, the feedback components, and the OA must be considered jointly to optimize the preamplifier design.

The photocurrent-to-voltage conversion is given by the ratio of the output voltage V to the input photocurrent I_P :

$$A_I = \frac{V}{I_P} = R \frac{1}{1 + G^{-1}} \quad (4.2)$$

where G is the loop gain. The photocurrent-to-voltage conversion is given by R , which is the signal gain, when $G \gg 1$ at the signal frequency. This is a very important design requirement for the analog control loop when low photocurrent measurement uncertainty is needed from a filter radiometer. For example, for a 0.02% photocurrent-to-voltage conversion uncertainty, G , should be 5000 or higher at the signal frequency (that corresponds to the electrical bandwidth of a DC mode measurement).

The DC loop gain is the product of A_0 and β_0 at low frequencies [19]:

$$G = A_0\beta_0 \quad (4.3)$$

where A_0 is the DC open-loop voltage gain of the OA and

$$\beta_0 = \frac{R_S}{R_S + R} \quad (4.4)$$

is the DC feedback attenuation. From Eqs. (4.2)–(4.4), the uncertainty of the photocurrent-to-voltage conversion depends on the photodiode shunt resistance. If a photodiode with high R_S is selected, the feedback attenuation β_0 will be close to unity, resulting in high G . Usually, the feedback resistor R is changed in decade increments to cover a wide dynamic signal range. The feedback resistors ranging from 1 k Ω to 100 G Ω are often used in preamplifiers to measure photocurrent (and hence radiant power) over a wide dynamic range.

A photocurrent meter (which is an analog control loop) can operate in the linear regime when these feedback resistors are used. At $R = 10^{12} \Omega$, the current-to-voltage conversion becomes non-linear. Using $R = 10^{11} \Omega$, the settling time of the output voltage V can be 2 min [19]. With the right design, R_S and R should be similar to each other and $R = 10 \text{ G}\Omega$ is usually enough to achieve very low noise in the output voltage V of the current meter [9]. With a maximum $R = 10 \text{ G}\Omega$ selection, the settling time will be less than 17 ms [19]. The loop-gain must be high enough at the signal frequency for all R selections to perform current-to-voltage conversions with the required low uncertainty.

The DC closed-loop voltage gain, A_{V_0} which is the reciprocal of β_0 (the inverse DC feedback attenuation),

$$A_{V_0} = \frac{R_S + R}{R_S} \quad (4.5)$$

determines the amplification of the input voltage noise V_{VN} of the OA. It is important to choose an operational amplifier for the photocurrent meter with low input voltage noise. Equations (4.2), (4.3), and (4.5) comprise the basic gain equations of the preamplifier.

In general, an OA has to be selected which satisfies the noise, drift, input current, and speed (bandwidth) requirements. The $1/f$ (peak-to-peak) noise

components of operational amplifiers between 0.1 and 10 Hz are available from data catalogs. The $1/f$ voltage noise is about $1\ \mu\text{V}$ for the OPA627BM and $2.5\ \mu\text{V}$ for the OPA111BM. The input current is about $5\ \text{pA}$ for the OPA627BM and about $1\ \text{pA}$ for the OPA111BM. The OPA128LM operational amplifier, which has a $1/f$ voltage noise of $4\ \mu\text{V}$ and a $1/f$ current noise about an order of magnitude lower than that of the other two models, can be used where smaller than $75\ \text{fA}$ input current is needed. This current will produce a small voltage drop on the high source resistance (the parallel connected R and R_S). When $R = 100\ \text{G}\Omega$ is selected, R_S can be close to $100\ \text{G}\Omega$ to obtain a large loop gain and low closed-loop voltage gain. However, care should be taken because the resistor noise can dominate the total noise at the output of the current meter and also the measurement will be very slow because of the long settling time. The high resistor noise can be decreased by making the electrical bandwidth very small. For slow DC measurements (the electrical bandwidth is smaller than 0.1 Hz) the amplifier noise is not available from data sheets; therefore, the total noise has to be measured [20]. In an optimum design, the resistor noise and the amplified $1/f$ noise are equalized for the output of the photocurrent meter at a given electrical bandwidth.

In Figure 4.7, V_{RN} is the Johnson (resistor) noise. This “white” noise shows up directly at the OA output (without any amplification). The current noise I_{IN} is caused by the fluctuation of the OA input current. Both I_{IN} and V_{VN} have “white” and $1/f$ noise components superimposed on each other.

The photocurrent I_P produces a shot noise I_{PN} , which is not shown in Figure 4.7. The current I_{PN} is converted to the OA output similar to I_P . This current noise component is $(2eI_P\Delta f)^{1/2}$, where e is the elementary electron charge, $1.60 \times 10^{-19}\ \text{C}$, I_P is the photocurrent, and Δf is the electrical bandwidth. A $10^{-14}\ \text{A}$ photocurrent produces an rms current noise of $I_{PN} = 7.1 \times 10^{-18}\ \text{A}$ at $\Delta f = 16\ \text{mHz}$, which corresponds to an integration time constant of 10 s.

At the OA output, the signal-produced voltage V has to be always much larger than the superimposed total noise voltage originating from the above four noise components. The signal-to-noise ratio at the current meter output has to satisfy the uncertainty requirement of a measurement.

The DC signal gain (V_0/I_P) of a preamplifier must be known or calibrated against high accuracy standards, such as resistor standards or current-source standards. In order to avoid tedious and limited accuracy signal-gain calibrations, the feedback resistors (R) should be purchased with a 0.01% uncertainty (tolerance) of their decade nominal values. Such resistors are commercially available from $1\ \text{k}\Omega$ to $100\ \text{M}\Omega$ with a resistance temperature coefficient of $10\ \text{ppm}/^\circ\text{C}$. The $R = 1\ \text{G}\Omega$ signal gain can be calibrated against the $R = 100\ \text{M}\Omega$ signal gain by measuring the same constant input current

(or optical radiation when the detector is connected to the preamplifier input). In order to utilize the 0.01% uncertainty of resistors R , a beam shutter should be used at the input of the filter radiometer. The output offset voltage of the preamplifier can be canceled out from the measurement by subtracting the dark reading (shutter closed) from the signal + dark reading (shutter open) at the output of the preamplifier (or the following digital voltmeter).

Usually, integrating-type digital voltmeters measure the preamplifier output voltage for the duration of 100 power line cycles (NPLC = 100) of 1.7 s to avoid long measurement times. An rms photocurrent noise floor of 1.5 fA was measured with NPLC = 100 on an optimized silicon photodiode current meter when R was selected to a maximum of 10^{10} V/A to avoid long settling times and high resistor noise [9]. Well-designed silicon photodiode current meters can be used as building blocks of high-performance filter radiometers, including photometers, pyrometers, and tristimulus colorimeters. These radiometers have a signal (radiant power or photocurrent) dynamic range of greater than 14 decades.

Photocurrent meters designed for AC measurements can measure weaker optical signals with shorter measurement times than DC photocurrent meters [9, 19]. A practical sensitivity limit in AC (chopped radiation) measurement mode with a 10 s integration time constant of 0.1 fA can be achieved [9]. The fundamental preamplifier gain equations (4.2), (4.3) and (4.5), are frequency-dependent. For AC measurements, the parallel C capacitors are to be calculated for all R selections to optimize the overall preamplifier performance.

4.3 Design Considerations of Irradiance Meters

The type of radiometric applications of the meter, as well as the calibration measurement conditions, need to be considered in the design and construction of an irradiance meter. In an ideal irradiance meter, the spectral irradiance responsivity $s_E(\lambda)$ is proportional to the projected area of the aperture in the measurement direction

$$s_E(\lambda) = A_d \cos(\alpha) s_{\text{avg}}(\lambda) \quad (4.6)$$

In Eq. (4.6), $s_{\text{avg}}(\lambda)$ is the average spectral power responsivity over the aperture area (A/W), A_d (m^2) the aperture area, and $\cos(\alpha)$ the projection of the aperture area in the measurement direction, where α is the angle between the incident radiant flux and the normal of the aperture plane. This is known as the cosine law of detector irradiance measurements. Note that the projected area is a maximum at perpendicular incidence ($\alpha = 0^\circ$) and zero at

$\alpha = 90^\circ$. If the incident beam is not parallel, α is no longer a constant, but can take a range of values depending on the measurement geometry. In this case, the integral of $\cos(\alpha)$ will be measured for all incident angles of the beam.

When irradiance is measured from an extended source, the angular responsivity of the irradiance meter has to follow the cosine function within the angular range determined by the size of the extended source and the detector aperture. In general, the FOV of the meter has to be larger than the largest convergence angle of the beam to be measured and overfills the aperture of the meter. This means that all of the radiation incident on the overfilled aperture of the irradiance meter must be measured by the under-filled active area of the detector.

Different kinds of apertures can be used in irradiance meters. The aperture edge should be always very thin to minimize radiation scatter. Also, the reflectance from the aperture surface should be well designed if the aperture reflectance is high. Otherwise, low-reflectance apertures should be used. Bi-metal apertures, such as black nickel-coated copper can be thin (e.g. 0.13 mm) and still convenient to use. A short bevel can be made between the aperture and the front surface of the radiometer to keep the stray radiation low.

One of the common approaches to the calibration of irradiance meters is to calibrate the spectral power responsivity of the irradiance meter and measure the aperture area. In this approach, the irradiance responsivity is equal to the spectral power responsivity times the measured aperture area. Irradiance measuring transfer standard radiometers that convert power responsivity into irradiance responsivity must have apertures of known area in front of the detector and good spatial uniformity.

The effective aperture area depends on the radiometer design and the geometry of the experimental setup and may not be equal to the geometrically measured aperture area. In some cases, the effective area depends on the beam geometry or source to instrument distance. To minimize the uncertainty associated with the effective area, in scale derivations and transfer to test artifacts, the measurement geometry should be specified. The geometrically measured aperture area can be equal to the effective aperture area if the beam incident on the instrument aperture is approximately parallel. In order to obtain this well-collimated beam shape, a "point-source"-type irradiance calibration geometry should be used.

Test irradiance meters that are calibrated by substitution against a reference irradiance meter do not need to have their aperture areas accurately measured. However, knowledge of the location of their reference planes is important if the measurement geometry changes. In general, the front surface of the aperture is the reference plane of an irradiance meter.

4.3.1 Mechanical and Optical Design

In order to understand design issues of irradiance measurements, consider ideal and real beam shapes and simplified detector input geometries shown in Figure 4.8. For an ideal irradiance meter, a thin aperture should be positioned on the active area of the detector. In this ideal case, the shape of the beam that overfills the aperture can change from a collimated, parallel beam to a large angle of β without any change in the irradiance responsivity. This measurement geometry is shown in Figure 4.8(a). The irradiance from different shapes of beams can be measured accurately with this ideal detector-input arrangement.

Typically, the detector has a protective window on the front and a spectrally selective filter is placed between the defining aperture and the reference detector. In most real instruments, therefore, a separation, or gap, exists between the aperture and the detector. The advantage of a point-source-like irradiation is that it produces a uniform irradiance with a well-collimated beam shape within the aperture of the irradiance meter. When this irradiance measuring geometry is used, shown in Figure 4.8(b), a separation or gap between the aperture and the detector does not affect the performance of the instrument.

If the incident beam is not collimated, multiple beam reflections between the detector surface and optical element between the detector and the aperture, or between the detector and the aperture itself can occur. This situation is shown in Figure 4.8(c) where the incident beam has a range of angles β . The reflectance pattern and the irradiance response can change with changing β . In this case, the instrument responsivity can be dependent on the geometry of the measurement. As a consequence, the instrument will no longer strictly follow the cosine law of detector irradiance measurements.

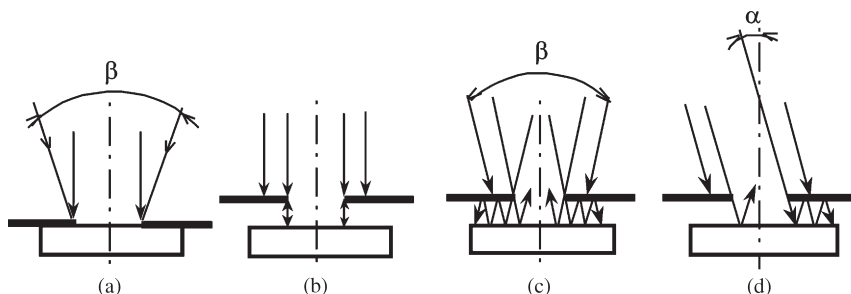


FIG. 4.8. Traditional input optics of irradiance meters with different incident beams. (a) Bare detector with a thin aperture on the top. (b) The parallel incident beam is perpendicular to the plane of the aperture. (c) The incident beam is converging. (d) The parallel incident beam is not perpendicular to the plane of the aperture.

A third situation is shown in Figure 4.8(d), where the parallel incident beam is no longer perpendicular to the aperture plane but is incident at an angle α relative to the normal of the aperture plane. In this situation, unwanted inter-reflections can also occur. Again, both the internal reflectance pattern and the responsivity deviation from the cosine function can be dependent on beam geometry.

For example, consider the angular responsivity of a real filter-type irradiance meter. The irradiance meter has a filter with a peak at 860 nm and a full-width, half-maximum bandpass of 60 nm. The separation between the aperture and the detector surface is approximately 4 cm. Figure 4.9 shows the responsivity of the radiometer as it was rotated around the center of its aperture in both the vertical and horizontal planes. The source was a Wi-41G lamp located 3 m away from the 4 mm diameter detector aperture. The responsivity deviation from the (ideal) cosine function is less than 0.05% within a beam convergence angle of $\pm 1^\circ$ (relative to the normal of the aperture plane). The deviation increases to 0.2% at about $\pm 2.5^\circ$. The two lobes located $\pm 2.5^\circ$ from normal incidence (0° radiometer rotation) where the responsivity is increased result from an increase in detector output signal caused by multiple internal reflections. It follows from the measurements that the geometry will affect the response of this instrument for beam geometries with convergence angles greater than 1° . To improve irradiance measurement uncertainty, better design is needed to increase the acceptance angle of irradiance measuring filter radiometers.

A properly designed irradiance meter follows the cosine law of detector irradiance measurements within a specified angular range or acceptance angle. This is known as the instrument's field-of-view (FOV). An irradiance

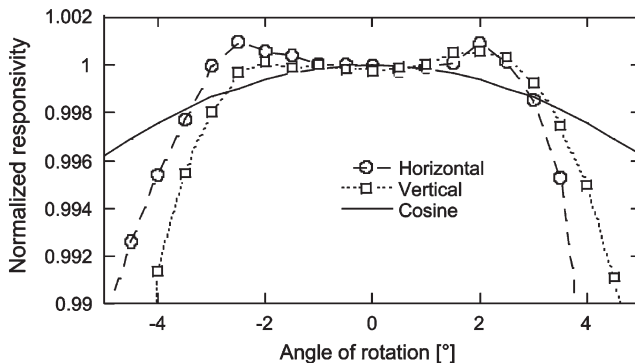


FIG. 4.9. Angular responsivity of an irradiance measuring filter radiometer where the aperture-filter-detector separations are large.

meter designed for high-accuracy measurements can only be used to measure sources within this FOV. The magnitude of the FOV depends on the application. The FOV should be small for “point source” and collimator measurements to reject radiation outside of the radiometer FOV. A larger FOV is needed for extended source measurements, especially if the source is close to the radiometer. Examples of different types of irradiance meters constructed with or without a diffuser, where the cosine responsivity is maintained within larger acceptance angles (or FOV), are discussed below.

4.3.2 Bandpass Type Irradiance Meters

The bandpass of an irradiance meter can be limited for different reasons. When broadband radiation is measured, the spectral responsivity of the irradiance meter must be standardized to obtain uniform measurement results. A typical example is the photopic filter for illuminance measurements. In other broadband source measurements, such as blackbody radiators, it makes the measurement simpler and faster if the spectral bandwidth of the detector is limited. For instance, it is possible to determine the temperature of a blackbody if its broadband radiation is measured only in a limited spectral range. In this case, the calibration of the bandpass radiometer is easier and faster, especially when tunable lasers are used for the radiometer calibration. The use of bandpass radiometers is especially important in the infrared, where the spectral range is much broader than in the visible.

4.3.2.1 *Irradiance meter design for single detectors*

In a well-designed irradiance meter, the input optical components (especially the detector and the aperture) are located close to each other to minimize the effects of internal reflections for different input beam geometries. Such an irradiance meter that can be built with different kinds of single element photodiodes is shown in Figure 4.4. Both filters and transmitting diffusers can be positioned in front of the photodiode. A thin aperture touches the front surface of the filter (or diffuser). The diffuser–input irradiance meter design issues will be discussed in Section 4.3.3. The aperture, filter, and photodiode are positioned as close to each other as possible.

The FOV of the irradiance meter, without using a diffuser, depends on the size of the detector, the gap between the detector and detector window, the thickness of the filter or filter combination, the gap between the filter and detector window, the gap between the filter and the aperture, and the size of the aperture. The gap between the filter and aperture should be equal to zero. In the best design, the aperture is thin and it touches the front surface of the filter. As the thickness of the filter or filter combination is given for a

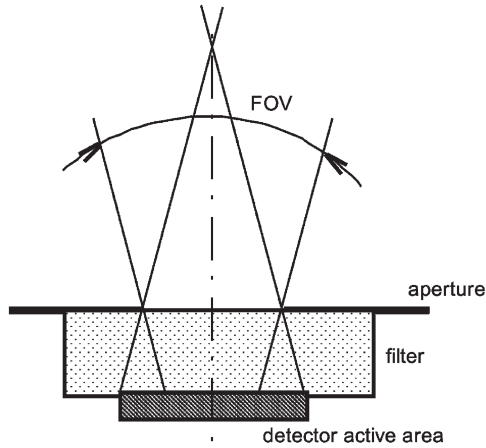


FIG. 4.10. FOV determination of a filter radiometer.

certain application, only the detector and aperture sizes can be selected to approach the desired FOV. Figure 4.10 shows the unvignetted FOV.

In the radiometer design shown in Figure 4.4, the radiometer has two independent temperature control loops. The first loop controls the temperature of the photodiode. Photodiodes with a thermoelectric cooler and a thermistor inside the sealed-can can be cooled to low temperatures for high-sensitivity applications. The bottom of the photodiode-can is attached to a copper base plate that delivers the dissipated heat to the heat sink of the housing. The second temperature control stabilizes the temperature of the filter/diffuser holder. The holder is pulled with three nylon screws against three thermoelectric coolers that are attached to the copper base plate through a copper ring. The leads of the TE cooler and the thermistor are attached through connectors and cable to an outside temperature controller. Selection of high stability and accurate temperature controllers is important to keep the measurement uncertainty low.

The photodiode leads are connected to the pins of a connector pair. The opposite side of the connector is mounted to the front panel of the bottom cylinder of the housing where the current-to-voltage converter (preamplifier) is located. Two printed circuit boards are used for the circuit components of the preamplifier including the operational amplifier, the feedback components, and the range switching reed relays. The rotary switch for gain control and two more connectors are located on the bottom plate of the housing. One connector connects the power supply to the radiometer head.

The second connector can be used to remote control the signal gains of the converter.

4.3.2.2 Filter-trap type irradiance meter

Internal reflections between the input aperture and the detector can be avoided if tunnel-trap detectors are used in place of the single element detectors. A significant advantage of a tunnel-trap detector is that no light is retro-reflected from the detector to the input aperture [21]. The scheme of a tunnel-trap detector is shown in Figure 4.11 [22]. An aperture on the front of the instrument defines the reference plane that is set to be in the same plane as the front panel. A five-channel, temperature-stabilized filter wheel is located between the aperture and the front of the tunnel-trap detector. The length of the filter packages is limited to 10 mm by the thickness of the filter wheel. A rotating knob located on the backside of the cover box is mounted on the shaft of the wheel for filter selection.

The space for the wheel, between the aperture and the trap detector, is about 12 mm. This separation does not decrease the FOV of this irradiance meter. An expanded view of the tunnel trap detector configuration is shown in Figure 4.12. Two 10×10 mm and four 18×18 mm silicon photodiodes, equivalent to the Hamamatsu S1337 model, were packed in a light trapping

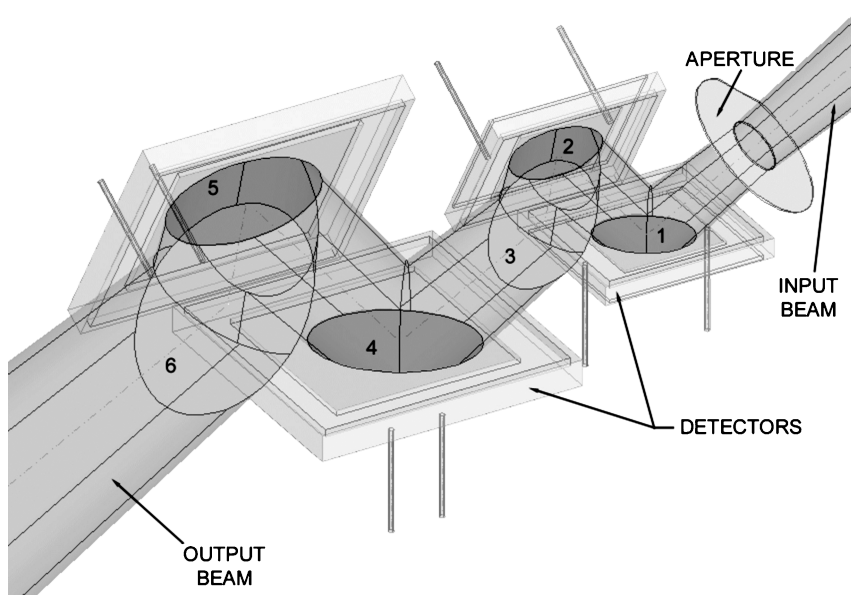


FIG. 4.11. Beam propagation inside the tunnel-trap detector.

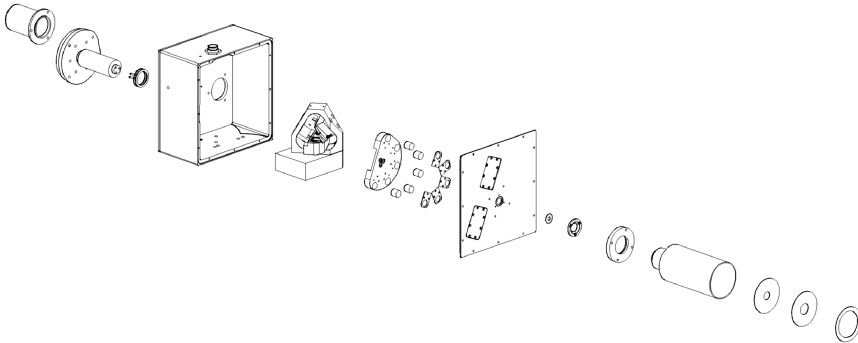


FIG. 4.12. Expanded view of the filter-trap radiometer layout.

arrangement. Temperature control for the photodiodes is not needed because the temperature coefficient of responsivity of these photodiodes is close to zero in the visible range and up to 950 nm. However, in order to minimize voltage gain for the input noise and drift of the operational amplifier in the photocurrent measuring circuit of the trap detector, the S1337 photodiodes were selected for high and equal shunt resistance. This selection was necessary because the six photodiodes were connected in parallel.

Figure 4.13 shows the normalized angular responsivity of the tunnel trap detector when it is equipped with a circular aperture of 5 mm diameter. The responsivity deviation from the expected cosine function is $<0.02\%$ within a 6° FOV. At 8° FOV, the deviation is still $<0.05\%$.

4.3.3 Diffuser-Type Irradiance Meters

A transmitting diffuser between the aperture and the detector is often used in the case where a relatively large FOV is needed. The diffuser can eliminate the changing reflectance patterns for different input beam shapes or source sizes. Glass diffusers or thin Teflon diffusers are often used for the visible and near-IR wavelength ranges. Diffusers can have very different angular transmittance characteristics. In principle, the goniometric Bidirectional Transmittance Distribution Functions (BTDF) of diffusers should be measured. For example, the BTDF of two different diffusers, a 3.2-mm-thick Spectralon diffuser and a 2.5-mm-thick flashed opal glass type diffuser, are illustrated in Figure 4.14 [23]. The BTDF was measured at 600 nm with normal beam incidence. The Spectralon diffuser showed a large forward scatter between $\pm 10^\circ$, while the normalized transmittance of the flashed opal glass was constant in a reasonably wide angular range. Figure 4.15 shows that the ideal Lambertian BTDF curve (solid circle) and the

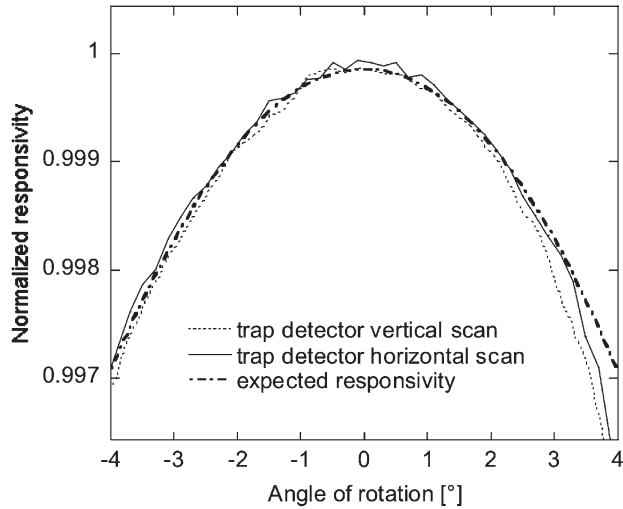


FIG. 4.13. Normalized angular responsivity of the tunnel-trap irradiance meter.

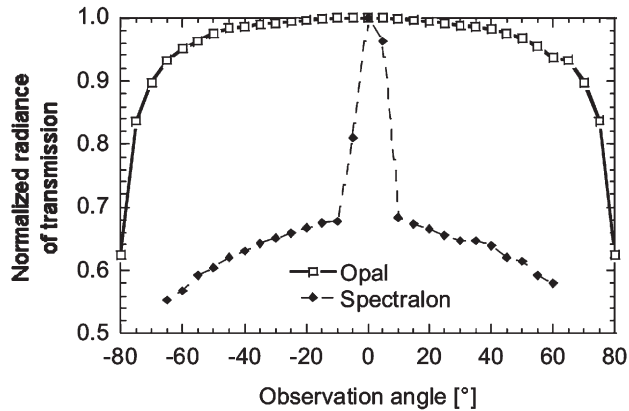


FIG. 4.14. BTDF of flashed opal glass and Spectralon diffusers at normal beam incidence.

measured flashed opal glass transmittance (dashed circle) curve are close to each other. Consequently, the flashed opal glass diffuser is the better choice for accurate irradiance meter developments when a relatively large FOV is required.

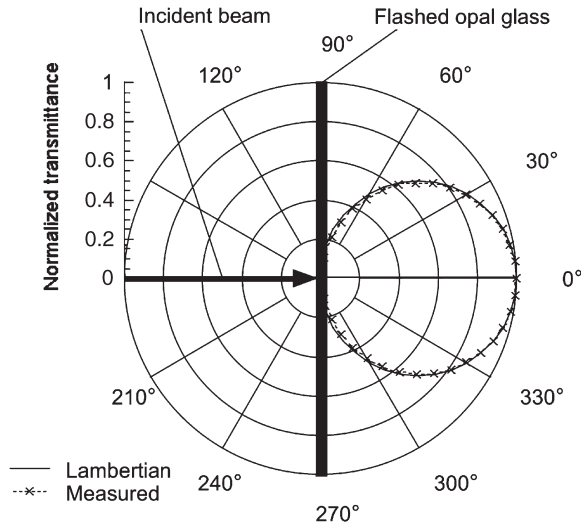


FIG. 4.15. Comparison of the angular transmittance distribution of a flashed opal glass diffuser (dashed) to an ideal Lambertian distribution (continuous).

The spectral dependence of the BTDF should also be considered; the BTDF of the above-measured flashed opal glass diffuser is significantly different at 1550 nm. Also, ground glass diffusers are not as good as flashed opal glass diffusers. They can be used only in the visible and within a smaller FOV. Unfortunately, there is not enough measurement data for different kinds of diffusers available. Therefore, goniometric characterizations should be made to select the best diffuser for a given application where low irradiance measurement uncertainty is needed.

Usually, optimization of the input geometry of diffuser-type irradiance meters is performed experimentally [24]. The angular responsivity depends upon the diameter of the aperture and the quality of the diffuser. When filters are used, they should be positioned between the diffuser and the detector and all three components (aperture, filter, and diffuser) should be included in the optimization. As the diffuse spectral reflectance and transmittance of the flashed opal glass diffusers is wavelength-dependent, the optimum cosine responsivity depends on the wavelength [24]. Consequently, the input geometry has to be optimized for the spectral distribution of the source to be measured.

To illustrate the effect of a transmitting diffuser application, the angular responsivity of a silicon irradiance meter using the design of Figure 4.4 built with selected aperture and diffuser to maintain the closest responsivity to the

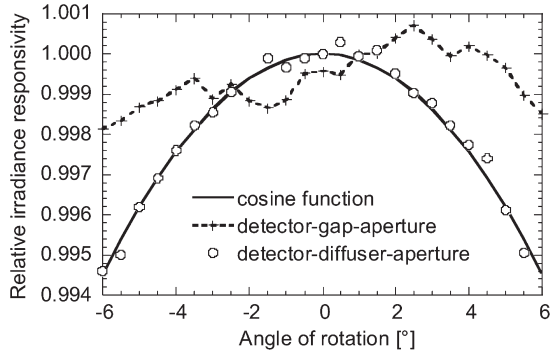


FIG. 4.16. Measured angular responsivity of a silicon irradiance meter with and without diffuser.

cosine function was measured with and without the diffuser. The dashed curve on Figure 4.16 shows how different the angular responsivity was from the ideal cosine function when a gap of about 7 mm was applied between the detector and the aperture. The open circles were obtained with the optimized aperture–diffuser combination. The small structure in the data points was caused by measurement noise including lamp instability and dust particles in the beam. The aperture was irradiated by a Wi-41G lamp from a distance of 3 m. The deviation from the cosine function is approximately equal to the measurement uncertainty of 0.03%. The deviation from the cosine function is still $<0.15\%$ at $\pm 12^\circ$ incidence angles.

A side effect of the cosine response optimization in diffuser-type irradiance meters is a change in the spatial responsivity distribution. The responsivity at the aperture edges will be smaller than in the center of the aperture. As an example, the response uniformity of the active area of a cosine optimized InGaAs irradiance meter is shown in Figure 4.17 when a 6.4 mm diameter aperture and a diffuser that transmits 40% at 1400 nm were selected. The spatial responsivity scans shown in Figure 4.17 were made at 1500 nm with a beam diameter of 1.1 mm. Each distance step of the scan was 0.5 mm along the horizontal x - and y -axis of the aperture relative to the aperture center. The y -axis shows the output signal of the InGaAs irradiance meter as normalized to the center position of the aperture. As shown in Figure 4.17(a), the responsivity decrease at the edge of the aperture can be as high as 20%. In Figure 4.17(b), the radiation scattered from the area surrounding the aperture can be seen for the same radiometer. Diffuser-input irradiance meters are not recommended for accurate radiant

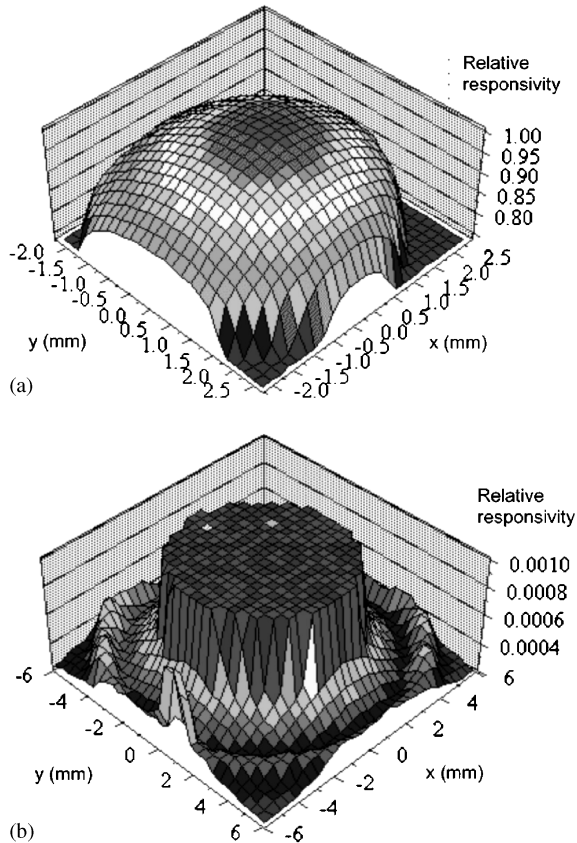


FIG. 4.17. Spatial responsivity distribution of a diffuser-input InGaAs irradiance meter. (a) the uniformity of the sensitive area; (b) the stray radiation around the radiometer aperture.

power measurements because of their high spatial non-uniformity of responsivity.

The effective area of an irradiance meter can be calculated as the ratio of the integrated irradiance responsivity to the radiant power responsivity in the center of the aperture. The effective area is utilized in flux transfers when the measured irradiance in the meter's aperture plane is transferred to another device, e.g., a sphere source to calibrate the radiance of its exit port [25]. Flux transfer is used when the measurement geometry is different from "point source" geometry. The result of the above spatial responsivity change will be a decreased effective aperture area for irradiance measure-

ments. Consequently, for irradiance meters with a diffuser input, measurement of the real, geometrical aperture area is meaningless.

The spectral characteristics of silicon and InGaAs irradiance meters are shown as well. The spectral characteristics were determined by the photodiode and the flashed opal glass diffuser used in the meters. In Figure 4.18, the spectral responsivity of the silicon and InGaAs photodiodes and the irradiance meters are shown. The magnitudes of the irradiance responsivities are similar for the two meters because the larger 8.0 mm diameter aperture of the Si meter produces higher irradiance responsivity than the smaller 6.4 mm diameter aperture of the InGaAs meter. Sources with either monochromatic or known (e.g., Planckian) spectral power distributions can be measured with these broadband irradiance meters. Similarly to InSb filter radiometers (as discussed in Section 4.3.5), use of bandpass filters between the diffuser and the detector makes it possible to measure the band-weighted irradiance of broadband extended sources.

4.3.4 Sphere-Type Irradiance Meters

When irradiance measurements are needed for even larger FOVs than those of diffuser-input irradiance meters, sphere-input irradiance meters can be used. The spatial uniformity of responsivity will not be degraded in well-designed sphere-input radiometers. Accordingly, these radiometers can be used for both irradiance and radiant power measurements with low meas-

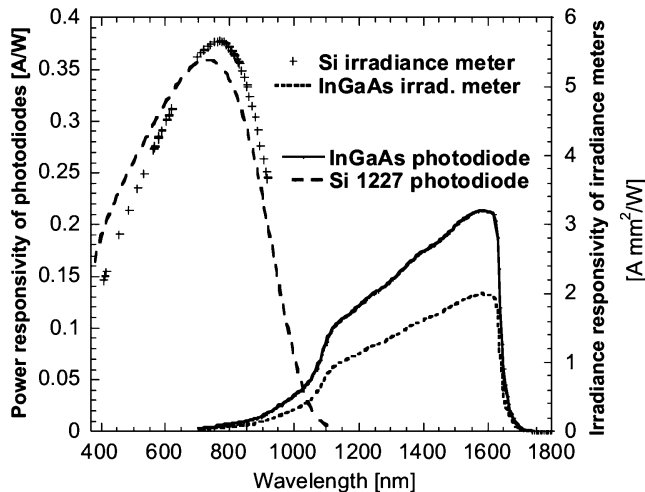


FIG. 4.18. Spectral responsivities of the Si and InGaAs photodiodes and the corresponding irradiance meters.

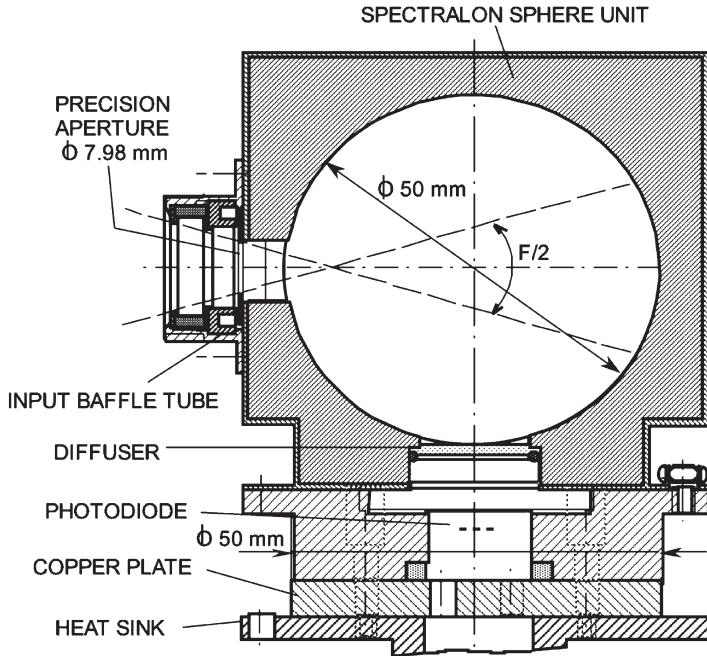


FIG. 4.19. Sphere-input irradiance meter.

urement uncertainties. Another advantage of sphere-input radiometers is that the entrance port with the input aperture can be made large to measure the incident radiant power of large-diameter beams.

As an example, the construction of a sphere-input irradiance meter is shown in Figure 4.19. In this radiometer, an integrating sphere is placed between the transmitting diffuser and the precision aperture. The sphere produces a spatially uniform input surface within the aperture area. In the design shown, the shape of the incident beam can change between $f/2$ and parallel. The FOV is limited by the precision aperture and the front aperture of the input baffle tube. The sphere wall is made of machined Spectralon (LabSphere, Inc., North Sutton, NH), a diffusing material with a reflectance of 99% over much of the visible. The irradiance on any part of the sphere wall is almost the same and proportional to the input flux (radiant power) penetrating the aperture. The plane-parallel transmitting diffuser, located in the exit port of the sphere, is part of the sphere wall. It is irradiated by the multiple reflections within the sphere. Any filters in the sphere-input irra-

diance meter should be located between the transmitting diffuser and the detector.

The efficiency of the flux transfer between the transmitting diffuser and the photodiode is determined from the geometry between them. The flux coupling efficiency, κ , for a 5-mm-diameter photodiode, an exit port diameter of 10.5 mm, and a separation between the diffuser and the photodiode of 6.5 mm, is equal to 8.5%. The efficiency, τ , of the 50 mm diameter sphere with its two ports and a transmitting diffuser with a transmittance of 36% located in the exit port, is equal to 21% [26, 27]. The overall radiant flux efficiency is $\kappa\tau = 0.018$, resulting in a signal attenuation of 56. The high-signal attenuation results in low radiometer responsivity. The decreased responsivity can be a disadvantage of sphere-input radiometers relative to the diffuser-input irradiance meters discussed above.

High throughput is sacrificed in sphere-input radiometers in order to achieve a spatially uniform receiving area and a large angular irradiance responsivity that follows the cosine function. Optimization of the spatial response uniformity and wide FOV, or large angular responsivity, in sphere-input radiometers are related tasks. Usually, the spatial non-uniformity is 0.1% or less, a factor of 3–5 better than that of the best quality silicon photodiodes. This is an important transfer standard feature for converting radiant power responsivity into irradiance responsivity.

The spatial response uniformity of the sphere-type irradiance meter of Figure 4.19 is shown in Figure 4.20. The scanning was made at 1500 nm by a 1.1-mm-diameter spot with 0.5 mm step sizes. The 0.1% maximum-to-minimum spatial responsivity change has a slope caused by the 90° asymmetrical arrangement of the entrance and exit ports. The spatial uniformity of

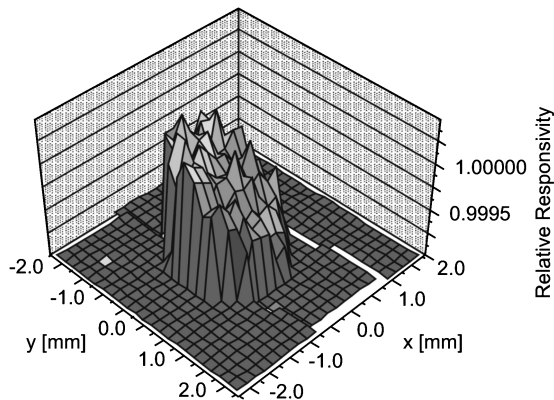


FIG. 4.20. Spatial uniformity of responsivity of a sphere-input Ge irradiance meter.

the responsivity could be further improved with a symmetrical multiple-detector arrangement. Spectralon has a significant retro-reflectance; at normal beam incidence to the aperture plane, more radiation leaves the sphere than at angular incidence. Therefore, for non-normal incident radiation, more reflected radiation is captured by the sphere and higher detector signal can be measured. Consequently, the angular responsivity will not follow the cosine response law. Instead, it will have two lobes similar to those of Figure 4.9. Tilting the plane of the input aperture can improve the situation. Even with a tilted aperture, the angular responsivity can be 0.2 to 0.3% different from the three-dimensional cosine function because of the asymmetric entrance and exit port arrangement. In order to obtain the best angular responsivity (the closest to the three-dimensional cosine function), either symmetrical entrance and exit port arrangements or additional baffles might be used.

With the right design, the angular range of sphere-input irradiance meters where the angular responsivity can follow the cosine function can be larger than that of diffuser-type irradiance meters. The FOV can be increased until the projected (from the incident radiation) and viewed (by the detector) areas will not overlap on the sphere wall. In the example of Figure 4.19, the $f/2$ corresponds to a FOV of about 30° . Time consuming selection of diffusers and apertures (like for the diffuser-type irradiance meters) and optimization for source wavelength is not needed here. Also, the highly non-uniform spatial responsivity of the cosine-optimized diffuser-type irradiance meters does not exist with the sphere-type irradiance meters.

4.3.5 Dewar-Type Infrared Filter Radiometers

The most popular IR detectors, InSb and HgCdTe (MCT), require operational temperatures close to 77 K for high radiometric performance. InSb detectors are usually photovoltaic (PV) devices (photodiodes) that can measure optical radiation from approximately 1 to $5.5\ \mu\text{m}$. MCT detectors are either PV or photoconductive (PC) and have a significant response to radiation over the range from 2 to $26\ \mu\text{m}$. The PC MCT detectors need bias currents. The cut-off wavelength can be tuned by changing the ratio of the composite material components of the detector. The spatial response non-uniformity of MCT detectors can be large. For low uncertainty measurements, they should be calibrated and used only in irradiance measurement mode to average out the spatial response non-uniformity [28]. In addition, the incident beam should be spatially uniform over the active area of the detector.

Filters used with the IR detectors discussed above should be maintained at low temperature as well to improve the noise floor by rejecting most of

the ambient background radiation from the detector. IR detectors are mounted in cryogenic dewars, where vacuum gives the temperature insulation between the cold detector and the warm external dewar wall. The detectors are mounted on a cold platform (finger). The position of the detector can be different after each cooling cycle. A typical change in the detector position, after a cooling cycle, is half a millimeter. Determination of the reference plane of a dewar-type irradiance meter with a low uncertainty is not easy because of this significant distance change relative to the front surface of the dewar. Also, a plane-parallel dewar window that is typically used to measure non-coherent radiation can shift the focus of a converging incident beam. These additional problems are to be taken into consideration in the design of the input optics when low measurement uncertainty is needed.

Using a cold low-pass filter, the upper cut-off wavelength of an InSb radiometer can be limited to, e.g. $2.5\ \mu\text{m}$. In this case, the background-radiation-produced signal-component can be significantly decreased. InSb radiometers with low background signal components can be operated in DC measurement mode. When an InSb radiometer has a wider spectral bandwidth in the longer wavelength region, the DC background signal component can be large. In this case, the signal to be measured must be chopped to distinguish the signal from the background component. A $0.2\ \text{pW}/\text{Hz}^{1/2}$ noise equivalent power (NEP) can be achieved in AC measurement mode when the background component of the detector signal is well attenuated using small FOV and narrowband cold filters [13].

In field calibrations, most IR detectors are used in irradiance (overfilled) mode [13] even if the responsivity scale was extended to the IR in radiant power measurement mode (e.g., using pyroelectric transfer standard detectors). Accordingly, a large IR detector with spatially uniform responsivity should be used for IR irradiance measurements. A 7-mm-diameter PV InSb detector with a shunt resistance of about $100\ \text{k}\Omega$ and a spatial response non-uniformity of less than 1% can be an optimum choice to obtain high irradiance responsivity and low preamplifier output noise. An aperture of known area (e.g., 6.4 mm diameter) can be positioned close (within 1 mm) to the detector to convert power responsivity into irradiance responsivity. As an example, the input design of an InSb filter radiometer is shown in Figure 4.21. This radiometer has a precision aperture of 6.4 mm diameter. It can measure both radiant power and irradiance. Only one cold filter is shown, located inside the cylindrical holder of the cold FOV limiter. Usually, at least two cold filters are needed to achieve 5–6 orders of magnitude blocking outside of the bandpass interval. The efficient blocking is needed when broadband sources (such as blackbodies) are measured. The cold filters and the small FOV produce a high background rejection. Using a second cold

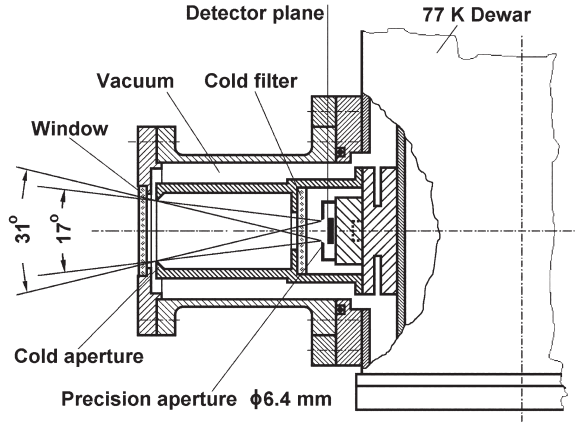


FIG. 4.21. Input-design of a Dewar-type InSb filter radiometer.

aperture in the FOV limiter, positioned 50 mm away from the precision aperture, a 17° unvignetted and a 31° total FOV was realized. With the input geometry shown, a maximum feedback resistor of $1\text{ M}\Omega$ could be used in the current-to-voltage converter attached to the backside of the dewar.

The InSb radiometer shown was calibrated in irradiance measurement mode. “Point source” like geometry was used to avoid changing internal reflectance patterns. The separation between the radiometer reference plane (which is different from the detector plane shown) and the source aperture was determined from a curve fit during the “point source” type irradiance measurements. The inverse square law was utilized in the curve fit. The measured irradiance responsivity of the InSb filter radiometer equipped with two bandpass filters of the same model is shown in Figure 4.22. The linear Y scale shows that the FWHM bandwidth is about 350 nm. The logarithmic Y scale illustrates the high out-of-band signal blocking. High-sensitivity InSb filter radiometers can be used for accurate irradiance calibration of infrared collimators even at very low irradiance levels.

4.4 Design Consideration of Radiance Meters

As discussed in Section 4.1, radiance meters use additional elements to define a measurement solid angle. These instruments measure a target area within a source. Wavelength-selective radiance meters are used to measure broadband sources such as blackbody radiators. As with irradiance meters, typically, the bandpass of these radiance meters is realized with filters. Ideally, the responsivity calibration method of a radiance meter has been con-

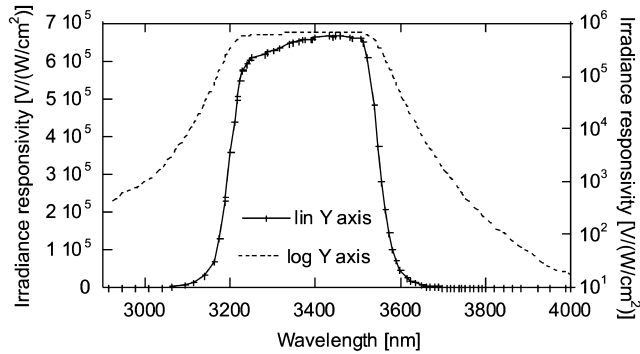


FIG. 4.22. Irradiance responsivity of an InSb filter radiometer.

sidered in its design. For example, when the spectral radiance responsivity is derived from the spectral power responsivity of the detector used in the radiance meter, the front geometry of the radiance meter must be well defined. In general, the signal component from the surrounding source-area outside the instrument's FOV should be highly attenuated by the radiance meter. Otherwise, measurement errors will occur that depend on the out-of-field area of the source.

4.4.2 Input Tube Attachment

A radiance meter can be an irradiance meter extended with a radiance measuring input optics. The simplest approach to produce a well-defined measurement angle is to place a second aperture at a fixed, known distance in front of the defining aperture in the irradiance meter. An input tube with two apertures, known as a Gershun tube [2], can be attached to the front of a filter radiometer for radiance mode measurements. Additional baffles are often placed between the two apertures to decrease unwanted signal components from stray and out-of-FOV radiation. The two apertures will determine the radiance measurement angle. Figure 4.23 shows the FOV scheme of the Gershun tube. The diameter of the detector aperture is d . This aperture in itself could be used for irradiance measurement. The diameter of the front aperture is D . The radiant power P entering the detector in radiance measurement mode is

$$P = L\omega_m A \quad (4.7)$$

where L is the radiance of the target surface measured by the meter, ω_m the

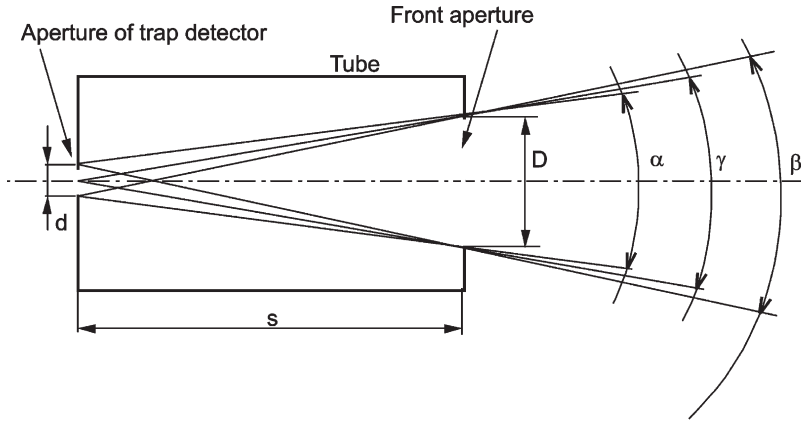


FIG. 4.23. Radiance measuring input tube attachment.

viewing solid angle (measurement angle) of the meter, and A the aperture area in front of the detector.

Using the symbols of Figure 4.23,

$$A = \frac{d^2 \pi}{4} \quad (4.8)$$

and

$$\omega_m = 2\pi \left(1 - \cos \frac{\gamma}{2}\right) \quad (4.9)$$

When $D = 11.29$ mm, and the separation s between the two apertures is 165 mm, the nominal (or effective) viewing angle can be calculated:

$$\gamma = 2 \tan^{-1} \frac{D}{2s} = 3.919^\circ \quad (4.10)$$

From the values given above and for $d = 5$ mm,

$$A = 0.1964 \text{ cm}^2, \quad \omega_m = 0.003674 \text{ s}$$

When the detector calibrated for power responsivity measures radiant power, the radiance of the target surface can be calculated from Eq. (4.7). Determination of ω_m from the nominal viewing angle γ is accurate only for small A_d . If we integrate the radiant power reaching the detector (from a uniform source of constant radiance L) for an ideal γ angle ($d = 0$) and the real case ($d > 0$), using the same detector aperture (A), the integrated difference (ideal radiance minus real radiance) will be -0.012% for $d = 5$ mm and -0.006% for $d = 3.5$ mm. These radiance (luminance) measurement

errors are very small. For a detector aperture with $d > 5$ mm, the integrated difference should be applied as a correction factor for the measured radiance.

The unvignetted FOV of the Gershun tube is

$$\alpha = 2 \tan^{-1} \frac{D - d}{2s} \quad (4.11)$$

For the above geometry (with $d = 5$ mm), α is 2.18° . The full radiance-measurement angle is

$$\beta = 2 \tan^{-1} \frac{D + d}{2s} \quad (4.12)$$

For the above tube design, $d = 5.65^\circ$. This full radiance-measurement angle must be smaller than the FOV of the detector. With this design, the unvignetted target-spot diameter (the plateau of the output signal) will be 40% of the full spot-diameter seen by the radiance/luminance meter.

The design of the baffle arrangement inside of the tube is shown separately in Figure 4.24 to illustrate the separation of rays from an extended source. Baffles B1 and B2 minimize the effect of stray light and reject radiation from light sources outside of the radiometer FOV. For simplicity, three rays are shown outside of the two FOV rays (producing α) to illustrate this situation for a large extended source.

For the tube design discussed above [24, 29], B1 had a diameter of 8.0 mm and it is located at a distance not too far from the detector aperture to avoid any clipping in the FOV. This baffle was fabricated with the same procedure as the other two FOV-limiting apertures. They were all made of copper, coated with black nickel. The aperture thickness is 0.13 mm. The position of B2 is not critical. It has a larger diameter and stops radiation entering the front aperture at large incidence angles.

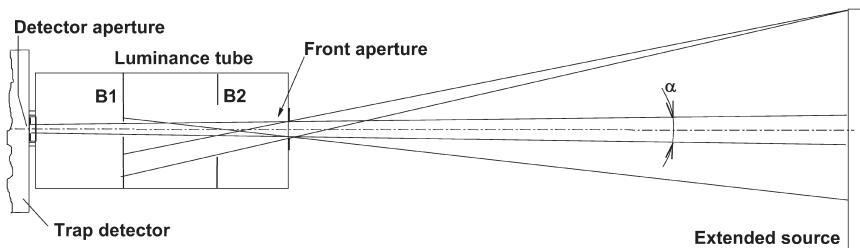


FIG. 4.24. Baffle arrangement (B1, B2) of the radiance/luminance tube in Figure 23.

4.4.3 Lens Input Optics

Lens input optics are used when small target areas are needed. As an example, Figure 4.25 shows the simplified optical/mechanical design of a filtered silicon radiance meter. The radiance input optics can be attached to the illuminance measuring base-unit using a threaded or bayonet-type mount. The beveled aperture mirror serves as a field stop, and it is positioned at the focus of a camera lens. Beveling minimizes stray radiation. The camera lens has a broadband antireflecting (AR) coating, resulting in high transmittance in the visible range. The surroundings of the source target area can be viewed through the eye-piece. The target radiation is imaged to the same center position of the photodiode through a second imaging lens system. The second imaging system produces a well-defined FOV and a very efficient out-of-FOV blocking. The original precision aperture, used for irradiance measurements, stays in front of the photodiode. It is underfilled (not used as a field stop) in radiance measurement mode. There is a dominant aperture stop in front of the second imaging lens system in order to keep the flux response of the optics constant for different target distances of the adjustable-focus camera lens. The filter package and the silicon photodiode are usually temperature controlled to 26°C. The filter-detector package can also be cooled when the cavity holding the filter and detector is sealed from the environment. This is the case for the instrument shown

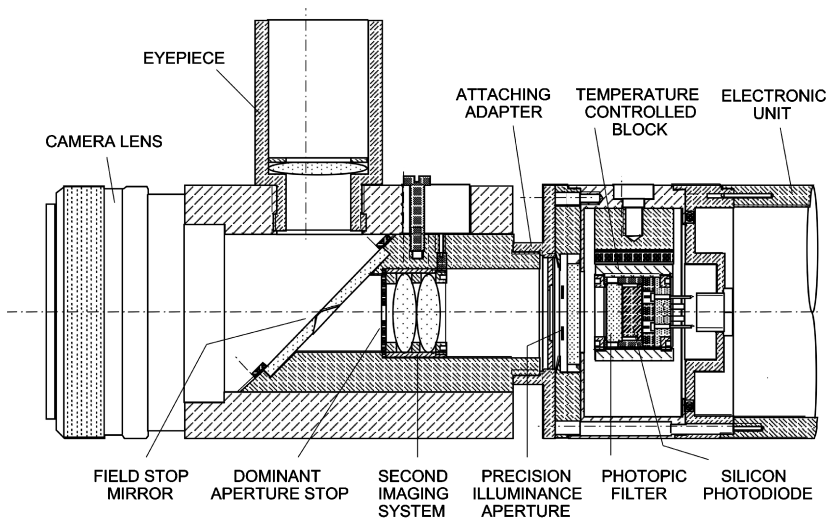


FIG. 4.25. Optical/mechanical scheme of a luminance optics attached to an illuminance meter.

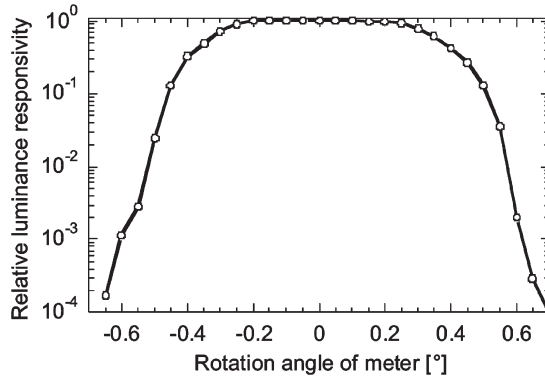


FIG. 4.26. Measurement profile of a radiance/luminance meter.

schematically in Figure 4.25. There is a window glued on the front of the temperature-controlled unit. The back of the filter–detector space is o-ring sealed to a case mount.

The relative responsivity of this radiance meter as a function of rotation angle of the meter is shown in Figure 4.26. A 3-mm-diameter source-spot, about 2 m away from the radiance meter, was measured. The pivot point of the luminance meter was the center of the field stop. The figure shows that the luminance measurement angle of the meter was about 1° and the out-of-FOV blocking was larger than four decades.

The responsivity change of the meter was 0.1% when the target distance was changed between 1 and 2 m. This change was equal to the relative measurement uncertainty associated to the results of the responsivity change measurements.

4.5 Calibration

A calibration relates the measured quantity from a radiometer, usually current or voltage, to the radiometric quantity being measured, e.g., radiance or irradiance, through the instrument’s responsivity. Often, establishment of traceability to the international system of units (SI) or to primary national or international radiometric standards is included as part of the calibration. Traceability is defined as the “property of the result of a measurement or the value of a standard whereby it can be related to stated references, usually national or international standards, through an unbroken chain of comparisons all having stated uncertainties.” [30] NIST has a

detailed policy outlining its role with respect to traceability [31]; many national metrology institutions have similar policies [32–34]. Determination of an instrument’s responsivity and an evaluation of the associated uncertainties are required in a calibration for an instrument to be traceable to NIST, other national metrology laboratories, and the SI.

The Mutual Recognition Arrangement (MRA) for national measurement standards and for calibration and measurement certificates issued by National Metrology Institutes (NMIs) was signed in 1999 by the directors of the NMIs of 38 member states of the Metre Convention and representatives of two international organizations. The objectives of the MRA were to establish the degree of equivalence of national measurement standards maintained by NMIs; to provide for the mutual recognition of calibration and measurement certificates issued by NMIs; and to thereby provide governments and other parties with a secure technical foundation for wider agreements related to international trade, commerce, and regulatory affairs [35].

Under the MRA, the metrological equivalence of national measurement standards are to be determined by a set of Key Comparisons chosen and organized by the Consultative Committees of the International Committee for Weights and Measures (Comite’ International des Poids et Mesures, CIPM) working closely with Regional Metrology Organizations (RMOs) [36]. An understanding of the measurement equation and an evaluation of the full uncertainty budget of the measurement by each participating laboratory are critical components of a Key Comparison.

A measurement equation is a mathematical expression describing the relationship between the measured quantity, the source radiometric quantity, and the instrument responsivity. In its simplest form, the measurement equation can be written as

$$i = \int L(\lambda)s(\lambda) d\lambda \quad (4.13)$$

where i is the measured output current, $L(\lambda)$ the source spectral radiance, $s(\lambda)$ the absolute radiance responsivity, and λ the wavelength. The detector output current is typically converted into voltage using a current-to-voltage converter, as described in Section 4.2.4. Of course, Eq. (4.13) could have been written in terms of source irradiance and absolute irradiance responsivity as well.

This simplified measurement equation ignores many of the detector characteristics that need to be quantified to establish the uncertainty in the calibration (and subsequent measurements of a source). Typically, the instrument’s response linearity, temperature dependence, polarization dependence, out-of-FOV blocking, and other parameters need to be measured.

In addition, the current-to-voltage converter and the multimeter used to measure the signal need to be characterized and their contribution to the overall uncertainty established. The uncertainty of the calibration source needs to be included in the uncertainty budget as well. Finally, both short-term stability (repeatability) and long-term stability (to monitor degradation in time) should be considered in establishing an instrument's combined standard uncertainty. Depending on the long-term stability, an instrument may need to be re-calibrated every 6 months, once a year, or once every several years. In general, until an instrument's behavior is well understood, a yearly calibration is recommended.

There are two types of uncertainty components, designated type A and type B. Type A uncertainties are evaluated using statistical methods while type B uncertainties are evaluated using models or other external information. The term "standard uncertainty" refers to an estimated standard deviation. Type B components of standard uncertainty are evaluated to be equivalent to one standard deviation. Assuming each uncertainty component is independent from the others (the components are uncorrelated), the combined standard uncertainty is the root sum square of the individual uncertainty components. Often, the different variables are not completely independent from one another, and correlations between these variables need to be taken into account [37, 38]. Correlations are discussed in detail in Chapter 6.

The expanded uncertainty is the product of the combined standard uncertainty and a coverage factor k , where the value of k is chosen based on the desired level of confidence. Typically the expanded uncertainty is reported with $k = 2$, corresponding to a confidence level of 95%. A confidence level of 95% means that there is a 1 in 20 chance that a measurement will fall outside the interval. A coverage factor $k = 3$ corresponds to a confidence level of 99%, meaning there is a 1% chance that a measurement will fall outside the stated interval. In reporting the uncertainty for a measurement, the components of standard uncertainty should be listed and their designation stated (A or B). It should be clear if the stated uncertainty is the combined standard or expanded uncertainty. If an expanded uncertainty is reported, the value of the coverage factor needs to be given as well.

Characterization of an instrument and an understanding and evaluation of all meaningful sources of uncertainty are critical for a proper calibration. A calibration without an associated uncertainty table is limited. The evaluation and expression of uncertainty is difficult and time-consuming; it is not unusual to have incomplete or inaccurate information in an uncertainty table. Determining how best to express a particular uncertainty component can be confusing. There are a variety of useful documents that provide

definitions and recommendations for describing and establishing the uncertainties encountered when calibrating a radiometer [39, 40].

There are two widespread calibration approaches for irradiance and radiance meters. In the first approach, the relative spectral responsivity (RSR) is measured and the system is calibrated using a standard source. This is the most common calibration approach. The relative spectral responsivity values are typically determined using broadband illumination sources combined with a tunable, spectrally selective instrument; lamp-monochromator systems are commonly used [41]. The second approach is to use a quasi-monochromatic source of known irradiance or radiance and directly determine the radiometer's absolute spectral responsivity (ASR). The absolute responsivity is determined in one step. Broadly tunable lasers are commonly used as a source in the second approach, with the lasers replacing the lamp-monochromator system described above. Using tunable lasers and integrating spheres with different size apertures, it is straightforward to achieve the correct beam geometry, flux level, and bandwidth [42–46].

Laser-based radiometric calibration facilities have been developed at several national metrology institutes, including NPL [44, 47], PTB [48], HUT [45] and NIST [42–44, 46, 49, 50]. A brief description is given of the NIST laser-based calibration facility, the facility for Spectral Irradiance and Radiance Responsivity Calibrations using Uniform Sources (SIRCUS) [42, 43]. In the SIRCUS facility, shown in Figure 4.27, high-power, tunable lasers are introduced into an integrating sphere producing uniform, quasi-Lambertian, high radiant flux sources. A wavemeter measures the wavelength of the radiation with an uncertainty of 0.01 nm or less; Fabry–Perot interferometers are used to monitor the mode stability of the laser radiation. Reference standard irradiance detectors, calibrated directly against national primary standards for spectral power responsivity, are used to determine the irradiance at a reference plane. The source radiance can be readily determined from the measurement geometry as well. Instruments are calibrated directly in irradiance or radiance mode with uncertainties approaching those available for spectral power responsivity calibrations. Ultimately, lasers determine the spectral coverage available in laser-based calibration facilities while the quality and characteristics of the reference standard detectors determine the achievable uncertainty.

In SIRCUS, the laser radiation is introduced into an integrating sphere, often using an optical fiber. Occasionally, a collimator coupled to the sphere is used as a calibration source. Speckle in the image from the source, originating from the coherent nature of the laser radiation, is effectively removed by either rastering the beam inside the sphere with a galvanometer-driven mirror or by placing a short length of optical fiber in an ultrasonic bath. Liquid light guides with a simple transducer attached to the side of the

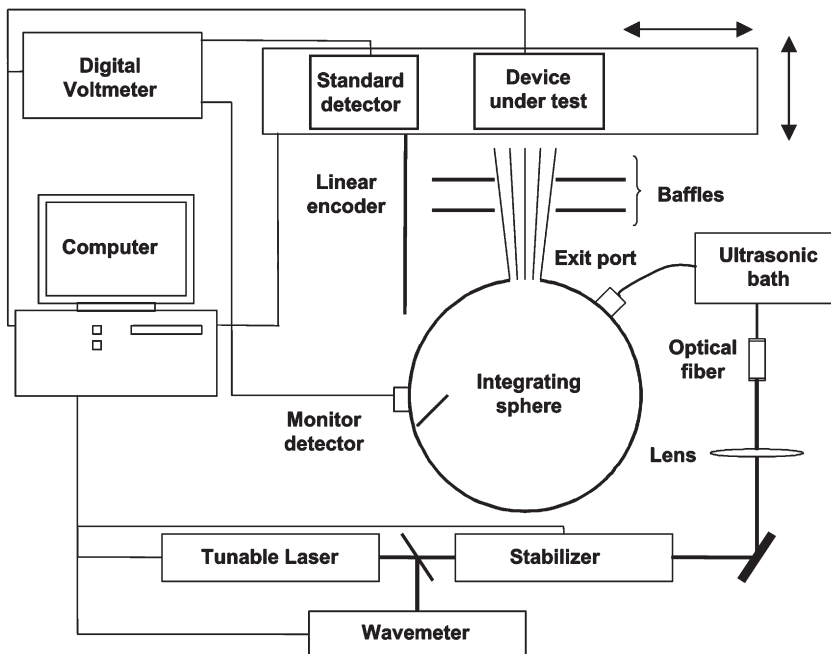


FIG. 4.27. Schematic diagram of the NIST SIRCUS laser-based calibration facility.

light guide also work well [48]. A monitor photodiode is located on the sphere to correct for any radiant flux changes in the sphere output between measurements with the reference instrument and the device under test. A number of different lasers are used to cover the spectral range from about 350 to 5000 nm, including continuous-wave (cw) dye lasers, solid-state Ti:sapphire lasers, as well as quasi-cw primary, doubled, tripled, quadrupled systems and optical parametric oscillator systems.

Different integrating spheres are used, depending on the radiometric calibration and the wavelength of calibration. Small-diameter integrating spheres—typically diameters of 25 to 50 mm—equipped with precision apertures with diameters ranging from 3 to 8 mm are typically used for irradiance responsivity calibrations. Larger diameter spheres—30 cm diameter—with 5–10 cm diameter exit ports are used for radiance measurements. The spheres are made of either sintered polytetrafluoroethylene-based coating [51] that has high diffuse reflectance from about 250 nm to 2.5 μm or diffuse gold [52] for calibrations from 1 to 20 μm . Typical irradiance levels at 1 m using a 25-mm-diameter integrating sphere with a 5-mm-diameter aperture range from approximately 1 to 10 $\mu\text{W}/\text{cm}^2$. Radiance

levels between 1 and 5 mW/cm²/sr are standard for a 300-mm-diameter sphere with a 75 mm output port. These radiance and irradiance levels can be continuously adjusted down to zero output, allowing for linearity measurements over many orders of magnitude. Note that the exit apertures are normally calibrated at the NIST facility for aperture area measurement [53].

The irradiance measurement equation, for “point-source” geometry, is

$$I(\lambda) = E_1(\lambda)d_1^2 = E_2(\lambda)d_2^2 \quad (4.14)$$

where I is the radiant intensity of the source at a given laser wavelength λ , E_1 the irradiance measured the irradiance standard transfer detector, located a distance d_1 from the source aperture, and E_2 the irradiance at the test detector’s reference plane, located a distance d_2 from the source aperture. E_2 is determined from the known irradiance E_1 multiplied by the ratio of the two distances, squared. The irradiance responsivity of the test detector is

$$s_E(\lambda) = \frac{i}{E_2} \quad (4.15)$$

where i is the current measured from the test device.

For radiance responsivity calibrations, the sphere radiance is the radiant intensity divided by the source aperture area and the radiance responsivity of the test radiometer is the measured current from the test instrument divided by the source radiance:

$$s_L(\lambda) = \frac{i}{L} \quad (4.16)$$

For both irradiance and radiance meters, a component approach to determine the relative spectral responsivity is commonly used. In this approach, the spectral power responsivity of the detector is measured, along with the transmittance or reflectance of all intervening optical elements, including filters. The relative spectral responsivity is then determined by multiplying the transmittance (or reflectance) of the individual components along with the detector responsivity. Differences between the component approach and system-level measurements can occur because of different measurement geometries and also because the former does not take into account inter-reflections between optical elements that are present in the complete system. For example, Figure 4.28 shows the calculated (by component) and measured relative spectral responsivity of three channels of a telescope, the Robotic Lunar Observatory (ROLO). Spectral shifts, changes in the spectral shape, and width are readily observable. The out-of-band response also differs significantly between the two approaches.

There is an additional approach for irradiance meters, called the scanned aperture method [45, 54–56]. In this approach, a beam much smaller than

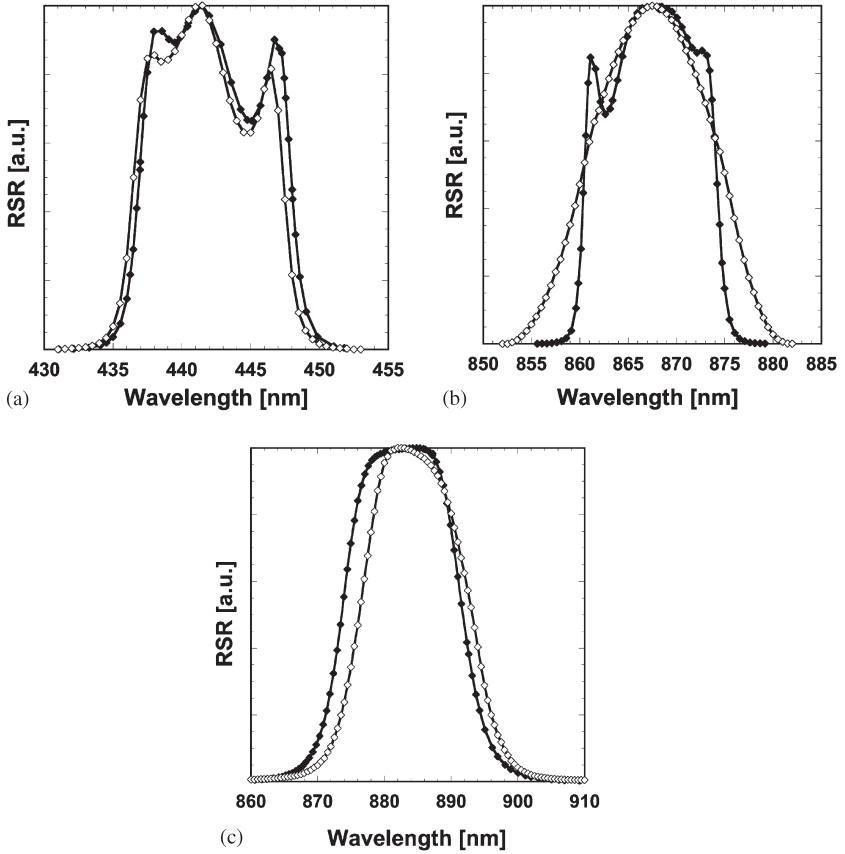


FIG. 4.28. Comparison between calculated (open diamonds) and measured (closed diamonds) relative spectral responsivity of three ROLO filter channels.

the defining aperture of the instrument is raster-scanned over the instrument's defining aperture. The effective aperture area can be determined by the ratio of the total signal summed over the scanned area (total irradiance responsivity) to the product of the total beam power $\phi(W)$ and the average spectral responsivity $\bar{s}(\lambda)$, within the active area of the defining aperture [54]:

$$A_{\text{eff}} = \frac{\sum i(x, y) \Delta x \Delta y}{\phi \cdot \bar{s}(\lambda)} \quad (4.17)$$

where Δx and Δy are the small steps taken when scanning over the aperture. The spectral irradiance responsivity is the product of the spectral power responsivity in the center of the aperture and the effective area. The scanned

TABLE 4.1. Comparison of the Operating Characteristics of a Laser-Based and a Lamp-Monochromator-Based Calibration Facility

Parameter	Laser-based facility	Lamp/monochromator
Optical power	300 mW	1 μ W
Bandwidth	< 0.001 nm	1 to 5 nm
Wavelength uncertainty	< 0.01 nm	0.1 nm
Power responsivity calibration	Yes	Yes
Uncertainty	0.1%	0.1%
Irradiance responsivity calibration	Yes	Yes
Uncertainty	0.1%	0.5%
Radiance responsivity calibration	Yes	No
Uncertainty	0.1%	
Digital imaging systems	Yes	No

aperture method using a lamp monochromator system has been compared with a direct calibration using tunable laser sources over the visible spectral region using an unfiltered silicon irradiance meter [42] and in the UV using 365 nm irradiance meters [54]. Calibrations using the two different approaches agreed to within 1%.

4.5.1 Comparison between Lamp-Monochromator and Laser-Based Calibration Approaches

The general characteristics of laser- [43] and lamp-based [41] calibration facilities at NIST are listed in Table 4.1. The high optical power available with laser-based calibration systems enables radiometers to be calibrated directly for either radiance or irradiance responsivity. The low-wavelength uncertainty of the laser is instrumental in reducing the calibration uncertainty for filtered instruments. Some of the advantages of the laser-based calibration approach are illustrated by the calibration of a Photo-Electric Pyrometer (PEP) used to radiometrically determine the temperature of a blackbody [57]. For accurate radiance temperature determinations, the instrument's spectral out-of-band responsivity needs to be measured as well as its in-band responsivity. The instrument is equipped with a narrow bandpass filter (~ 1 nm FWHM) for spectral selectivity. Figure 4.29 shows the relative spectral responsivity of the PEP determined on SIRCUS compared with the relative spectral responsivity determined using a conventional lamp-monochromator system. As shown in Figure 4.29(a), the spectral responsivity measured with the lamp-monochromator system is dominated by the spectral bandwidth of the source, and deconvolution of the spectrum using the source slit scatter function is required. In contrast, the fine detail in the

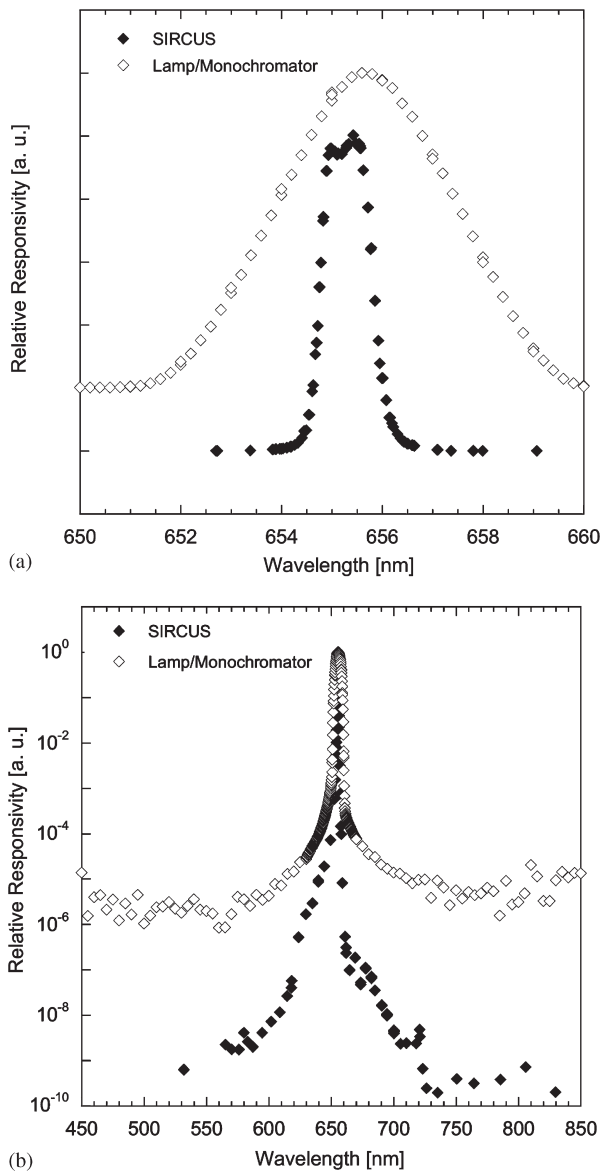


FIG. 4.29. Relative spectral responsivity of the PEP measured on the laser-based and the lamp-monochromator-based facilities at NIST: (left) linear scale; (right) log scale.

spectral responsivity is easily measured with the tunable laser facility because of the monochromatic nature of the source. Note that there are several overlying data points at each wavelength along both the rising and falling edges, demonstrating the extreme wavelength stability and repeatability of the laser-based calibration. Because of the low flux, the out-of-band responsivity is limited to approximately 10^{-6} with the lamp-monochromator system (Fig. 4.29(b)). In contrast, the out-of-band responsivity can be measured to the 10^{-9} level in the laser-based facility.

Because of the coherent, narrowband nature of the laser radiation, oscillations or interference fringes in the responsivity arising from multiple reflections from surfaces of different optical components can occur. For example, Figure 4.30 shows the responsivity of a filter radiometer determined using a laser-based source. What appears to be “noise” in the in-band responsivity (Fig. 4.30(a)) is shown to be interference fringes by examining a narrow spectral region in detail and tuning the excitation wavelength in very small increments (Fig. 4.30(b)). Interference fringes are often observed when calibrating radiometers with windowed detectors. The interference fringes can be greatly reduced or eliminated by proper design of the radiometer keeping the calibration in mind, e.g. through the use of wedged windows.

4.5.3 Traceability to SI units

Historically, radiometric and photometric measurements and calibrations have been based on standard sources. Spectral radiance and irradiance quantities as well as photometric quantities were based on the properties of blackbody radiators. Beginning in the early 1970s, detectors began to be incorporated into photometric and radiometric standards [58]. These developments were facilitated by improvements in detector material properties (especially silicon detectors) and devices [59] along with the development of high-accuracy electrical substitution radiometers that operated at cryogenic temperatures [60, 61]. Derivations of radiometric and photometric quantities using detectors can often be maintained with lower uncertainties than with source-based primary standards. Consequently, most national metrology institutions have moved or are moving toward detector-based measurements of radiometric, photometric, and colorimetric quantities [58].

The SI unit that serves as the base for all photometric quantities is the candela. The candela was defined in 1948, based on the radiation emitted from a platinum blackbody operating at the freezing-point temperature of molten platinum [62]. In 1979, the candela was redefined in terms of optical power as [63]

The candela is the luminous intensity, in a given direction, of a source that emits monochromatic radiation of frequency 540×10^{12}

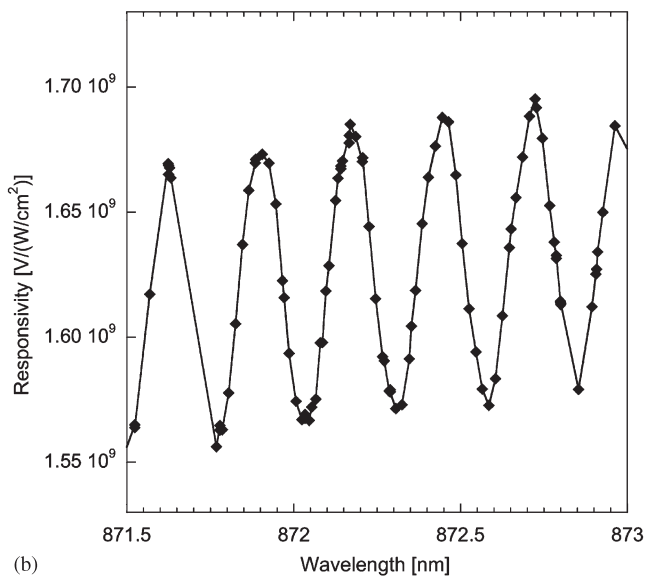
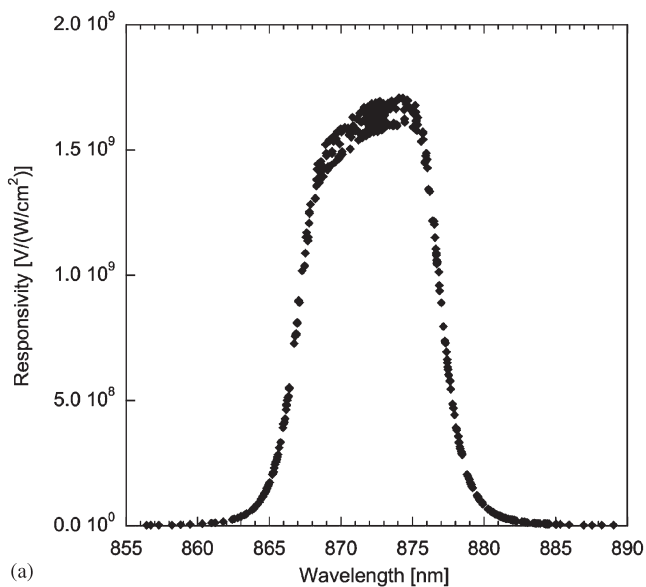


FIG. 4.30. (a) Absolute spectral responsivity of a filter radiometer measured in a laser-based calibration facility. (b) Expanded view of a small spectral region, demonstrating the presence of interference fringes.

hertz and that has a radiant intensity in that direction of (1/683) watt per steradian.

The luminous intensity is the luminous flux emitted per unit solid angle in a given direction; the luminous flux is the radiant flux weighted by the photopic efficacy function, $V(\lambda)$. This definition of the candela in terms of optical power and a recognized weighting function provided the opportunity to base the measurement of photometric quantities on the properties of well-designed detectors. NIST and other national laboratories moved rapidly to establish detector-based photometric scales [62–64]. The implementation of the detector-based photometric scale reduced the uncertainty in the derivation of photometric quantities by factor of two at NIST [65]. International Key Comparisons of luminous intensity, luminous flux and luminous responsivity were held in the 1990s; results are available from the Bureau International des Poids et Mesures (BIPM) [35]. Refer to Chapter 7 for additional information on photometry.

Lamp-illuminated integrating spheres or lamp standards of spectral irradiance are often used to calibrate radiometers. The spectral radiance values assigned to lamp-illuminated integrating sphere sources (ISSs) have been determined by reference to the gold-point and other fixed-point blackbodies and the international temperature scale of 1990 (ITS-90) [66, 67]. Given a source spectral radiance $L(\lambda, T)$ and a filter radiometer's absolute spectral responsivity, a comparison can be made between predicted and measured signal from the filter radiometer when measuring the source, with the predicted signal S_p given by

$$S_p = \int s(\lambda)\varepsilon L(\lambda, T) d\lambda \quad (4.18)$$

where ε is the emissivity of the blackbody radiator. For a source such as a blackbody, there exists a well-known relationship between the temperature and the spectral radiance, given by Planck's equation [1, 50].

The spectral responsivities of filter radiometers calibrated on the laser-based calibration facility are determined by direct substitution against a cryogenic radiometer. The irradiance responsivity is determined by measuring a precision aperture that is installed on the front surface of the radiometer. To determine the source radiance, the source exit port area and the distance between the source and detector apertures needs to be measured. Consequently, measurement of a blackbody source radiance using filter radiometers calibrated against, or traceable to, a cryogenic radiometer is based on electrical substitution radiometry and dimensional metrology, independent of the ITS-90 definition of the Kelvin. By comparing the predicted vs. measured signals when the filter radiometer measures the radi-

ometric output of a fixed-point blackbody (e.g. a gold-point blackbody) whose temperature is defined by ITS-90, the ITS-90 temperature scale can be compared to the SI units of length (m) and power (W).

Shortly after the development of tunable dye lasers in the late 1970s, an intercomparison was made between electrical-substitution-based and blackbody-based radiometry using silicon filter radiometers to measure a tungsten halogen lamp [68]. Spectroradiometric determinations of the thermodynamic freezing and melting temperatures of gold, silver, and aluminum blackbodies followed [1, 50]. In 1991, an approach was outlined to derive the radiation temperature scale from 1000 to 3000 K using filter radiometers calibrated for absolute spectral responsivity against standard detectors traceable to a cryogenic radiometer [69]. The approach was realized at NIST in 2000 with the development of the detector-based spectral irradiance scale [70]. In Figure 4.31, the combined expanded ($k = 2$) uncertainties of the 1990 (source-based) and the 2000 (detector-based) spectral irradiance scale realizations are shown. The detector-based spectral irradiance scale has an uncertainty factor of 2 or more less than the ITS-90

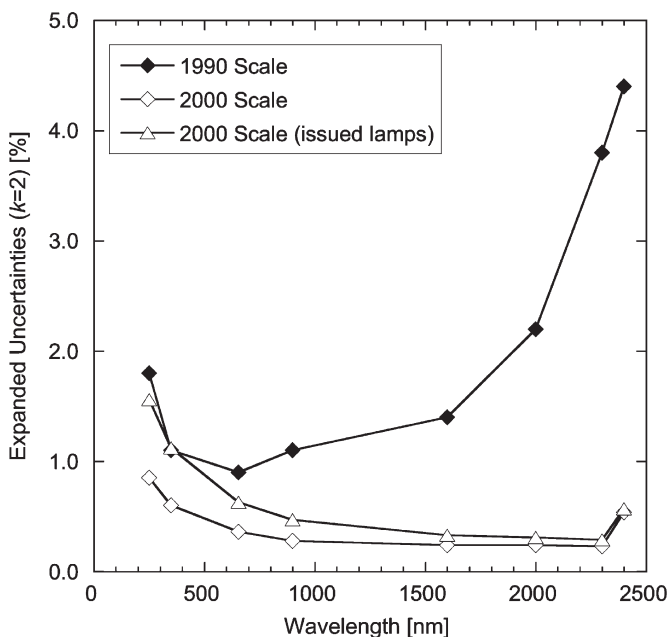


FIG. 4.31. Comparison of the expanded ($k = 2$) uncertainties of the NIST 1990 and 2000 spectral irradiance scale realizations.

(source-based) irradiance scale. The reduction in uncertainty increases up to a factor of 10 in the infrared spectral region.

A pyrometer—denoted the Advanced Pyrometer-1 (AP1)—was built at NIST to radiometrically measure blackbody temperatures [29, 71]. Spectral selection is achieved using two narrowband interference filters with nominal center wavelengths at 650 nm and an additional infrared blocking filter to suppress radiation beyond 800 nm. The filters are temperature-stabilized near room temperature and the hermetically sealed silicon photodiode has a two-stage thermo-electric cooler for operation at -15°C . It has a NEP of 10 fW. The AP1 was calibrated for absolute spectral radiance responsivity on SIRCUS. As shown in Figure 4.32, it has a peak responsivity between 647 and 652 nm, a full-width half-maximum bandwidth of about 10 nm and out-of-band blocking better than 10^{-7} . Interference fringes with a magnitude

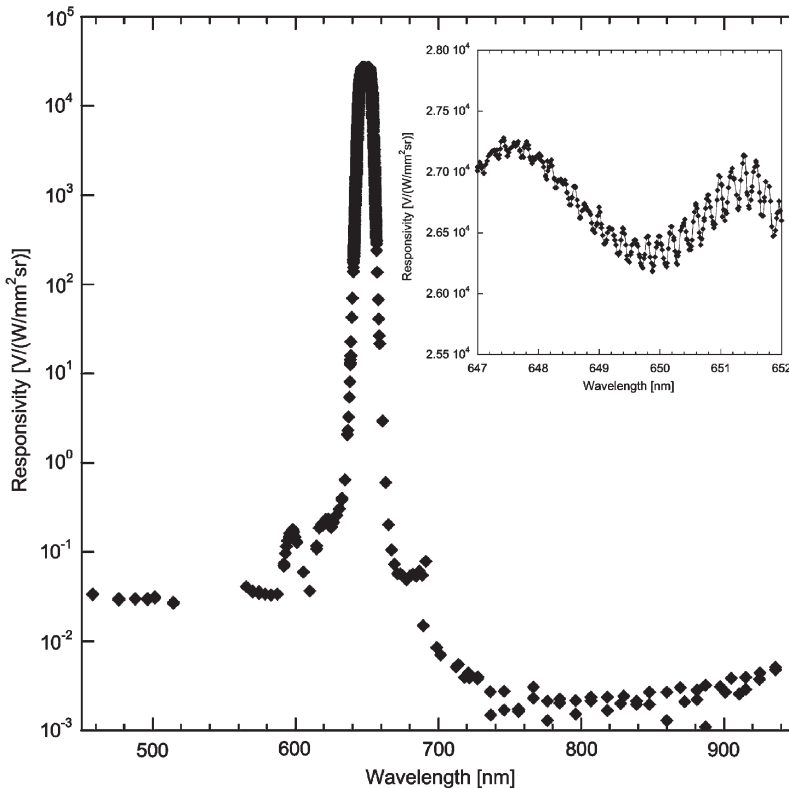


FIG. 4.32. AP-1 responsivity measured on SIRCUS. Inset shows interference fringes in the measured absolute spectral responsivity.

of 0.5% were observed in the responsivity (see Figure 4.32, inset). The absolute spectral responsivity was therefore measured with 0.03 nm resolution. The API subsequently measured the melt and freeze cycles of silver and gold fixed-point blackbodies. The signal from the API is converted to temperature using Planck's equation [72].

The noise-equivalent temperature at the gold (and silver) freezing temperature is ≈ 2 mK, and the noise will not be the dominant component of the total temperature uncertainties. The expanded uncertainty ($k = 2$) in the radiometric measurement of the gold (or silver) freezing-point blackbody is approximately 0.15%. The radiometric uncertainties can be related to the uncertainties of the temperature determinations from the derivative of the Wien approximation, which shows the relationship between the uncertainty in radiance, L , to the uncertainty in blackbody temperature, T :

$$\frac{\Delta L}{L} = \frac{c_2}{\lambda} \frac{\Delta T}{T^2} \quad (4.19)$$

In Eq. (4.19), c_2 is the second Planck's constant, and λ is the wavelength. Using Eq. (4.19), an uncertainty of 0.1% in radiance responsivity at 650 nm will lead to a temperature uncertainty of 80 mK in the measurement of the temperature of the gold-point blackbody.

In the ITS-90, the assigned temperatures for the Al, Ag, and Au freezing points result from thermometry using ratio pyrometry from the mean of two different and conflicting constant-volume gas thermometry measurements at lower temperatures. There are thermodynamic temperature uncertainties of the freezing points of the primary metal blackbodies that arise primarily from the uncertainties in the lower temperature gas thermometry. Although the thermodynamic temperature uncertainties of the Au- and Ag-freezing temperatures are not stated in the ITS-90, they have been listed in Table 4.2 for comparison. Radiometric determinations of the Au- and Ag-freezing points reported by Fox et al. from the NPL in 1991 [1] are included as well.

Note that the uncertainties in the freezing temperatures of primary gold and silver-point blackbodies determined using thermodynamic measurements (the ITS-90) and radiometric measurements, shown in Table 4.2, are similar. Laser-based calibration facilities can be used to calibrate optical

TABLE 4.2. Summary ITS-90 and Spectroradiometric Determinations of Ag- and Au-Black-body Freezing Point Temperatures

Material	$T_{\text{ITS-90}}$ (K)	$u(k=2)$ (K)	T_{API} (K)	$u(k=2)$ (K)	T_{NPL} (K)	$u(k=2)$ (K)
Ag	1234.93	0.080	1234.956	0.106	1235.009	0.088
Au	1337.33	0.100	1337.344	0.121	1337.300	0.098

pyrometers directly, eliminating the dependence on a blackbody and the ITS-90. As discussed in Yoon et al. [71], this can result in greatly reduced uncertainties in the measurement of thermal sources at higher temperatures.

Irradiance and radiance scales based on ITS-90 and electrical substitution radiometry have been intercompared, both within a calibration facility [49, 68, 73] and between laboratories [74]. The two approaches agreed to within 0.5% over a wide temperature range.

4.6 Conclusions

Modern, low-uncertainty detector-based reference scales for radiometric calibrations are those of spectral irradiance responsivity. Reference spectral irradiance responsivity scales can be realized by radiant power/irradiance measuring trap detectors in the silicon wavelength range. These silicon trap detectors are the highest-level transfer standards that can be used as reference detectors for all low-uncertainty spectral responsivity calibrations in the ultraviolet, visible and near-infrared range. For specific measurement tasks and responsivity scale propagations, filter radiometers can be used as transfer/working standards. These filter radiometers can be developed for many different measurement configurations. They are robust, simple to use, and can measure different radiometric (or photometric) quantities, such as power, irradiance, or radiance (luminous flux, illuminance, or luminance). The filter radiometers can be calibrated against the highest level (cryogenic radiometer or trap detector) standards (with the simplest possible geometry) and used as reference devices for other calibration facilities or field measurements. The result is a short calibration chain with low measurement uncertainty.

References

1. N. P. Fox, J. E. Martin, and D. H. Nettleton, Absolute spectral radiometric determination of the thermodynamic temperatures of the melting/freezing points of gold, silver and aluminium, *Metrologia* 28, 357–374 (1991).
2. R. McCluney, “Introduction to Radiometry and Photometry.” Artech House, Norwood MA, 1994.
3. A. Dahlback, Measurements of biologically effective UV doses, total ozone abundances, and cloud effects with multichannel, moderate bandwidth filter instruments, *Appl. Opt.* 35, 6514–6521 (1996).

4. C. Wehrli, Calibrations of filter radiometers for determination of atmospheric optical depth, *Metrologia* 37, 419–422 (2000).
5. T. C. Larason and C. L. Cromer, Sources of error in UV radiation measurements, *J. Res. Natl. Inst. Stand. Technol.* 106, 649–656 (2001).
6. G. Eppeldauer, “Optical Radiation Measurement with Selected Detectors and Matched Electronic Circuits Between 200 nm and 20 μm .” NIST Technical Note 1438, NIST, 2001.
7. G. Eppeldauer, Temperature monitored/controlled silicon photodiodes for standardization, *Proc. SPIE* 1479, 71–77 (1991).
8. T. R. Gentile, J. M. Houston, and C. L. Cromer, Realization of a scale of absolute spectral response using the NIST high-accuracy cryogenic radiometer, *Appl. Opt.* 35, 4392–4403 (1996).
9. G. Eppeldauer, Noise-optimized silicon radiometers, *J. Res. Natl. Inst. Stand. Technol.* 105, 209–219 (2000).
10. K. Solt, et al., PtSi-n-Si Schottky barrier photodetectors with stable spectral responsivity in the 120–250 nm spectral range, *Appl. Phys. Letts.* 69, 3662–3664 (1996).
11. G. Eppeldauer, Electronic characteristics of Ge and InGaAs radiometers, *Proc. SPIE* 3061, 833–838 (1997).
12. G. P. Eppeldauer, A. L. Migdall, and L. M. Hanssen, InSb working standard radiometers, *Metrologia* 35, 485–490 (1998).
13. G. P. Eppeldauer and M. Racz, Spectral power and irradiance responsivity calibration of InSb working standard radiometers, *Appl. Opt.* 39, 5739–5744 (2000).
14. J. Lehman, et al., Domain-engineered pyroelectric radiometer, *Appl. Opt.* 38, 7047–7055 (1999).
15. G. P. Eppeldauer, M. Racz, and L. M. Hanssen, Spectral responsivity determination of a transfer-standard pyroelectric radiometer, *Proc. SPIE* 4818, 118–126 (2002).
16. P.-S. Shaw, et al., The new ultraviolet spectral responsivity scale based on cryogenic radiometry at Synchrotron Ultraviolet Radiation Facility III, *Rev. Sci. Instrum.* 72, 2242–2247 (2001).
17. “CIE Publication 69: Methods of Characterizing Illuminance Meters and Luminance Meters.” Commission Internationale de L’Eclairage (CIE), Vienna, 1987.
18. G. P. Eppeldauer and M. Racz, Design and characterization of a photometer-colorimeter standard, *Appl. Opt.* 43, 2621–2631 (2004).
19. G. Eppeldauer, Chopped radiation measurement with large area Si photodiodes, *J. Res. Nat. Stand. Technol.* 103, 153–162 (1998).
20. G. Eppeldauer and J. E. Hardis, Fourteen-decade photocurrent measurements with large-area silicon photodiodes at room temperature, *Appl. Opt.* 30, 3091–3099 (1991).

21. J. L. Gardner, Transmission trap detectors, *Appl. Opt.* 33, 5914–5918 (1994).
22. G. P. Eppeldauer and D. C. Lynch, Opto-mechanical and electronic design of a tunnel-trap Si- radiometer, *J. Res. Nat. Stand. Technol.* 105, 813–828 (2000).
23. G. Eppeldauer, Near infrared radiometer standards, *Proc. SPIE* 2815, 42–54 (1996).
24. G. Eppeldauer, M. Racz, and T. Larason, Optical characterization of diffuser-input standard irradiance meters, *Proc. SPIE* 3573, 220–224 (1998).
25. J. H. Walker, R. D. Saunders, J. K. Jackson, and D. A. McSparron, Spectral irradiance calibrations, in “NBS Measurement Services.” U.S. Nat. Bur. Stand., 1987.
26. D. G. Goebel, Generalized integrating sphere theory, *Appl. Opt.* 6, 125 (1967).
27. “A Guide to Integrating Sphere Theory.” www.labsphere.com, Labsphere Inc., No. Sutton NH, 2004.
28. H. Gong, L. M. Hanssen, and G. P. Eppeldauer, Spatial and angular responsivity measurements of photoconductive HgCdTe LWIR radiometers, *Metrologia* 41, 161–166 (2004).
29. D. W. Allen, G. P. Eppeldauer, S. W. Brown, E. A. Early, B. C. Johnson, and K. R. Lykke, Calibration and characterization of trap detector filter radiometers, *Proc. SPIE* 5151, 471–479 (2003).
30. International Organisation for Standardization (ISO), “International Vocabulary of Basic and General Terms in Metrology.” 1993. QA :2
31. <http://ts.nist.gov/traceability>.
32. National Physical Laboratory, United Kingdom, www.npl.co.uk.
33. Physikalisch Technische Bundesanstalt, Germany, www.ptb.de.
34. National Research Council, Canada, www.nrc.ca.
35. Bureau International des Poids et Mesures (BIPM), www.bipm.org.
36. BIPM Key Comparison Database, kcdb.bipm.org.
37. J. L. Gardner, Correlated color temperature-uncertainty and estimation, *Metrologia* 37, 381–384 (2000).
38. J. L. Gardner, Correlations in primary spectral standards, *Metrologia* 40, S167–S176 (2003).
39. International Organisation for Standardization (ISO), “Guide to the Uncertainty in Measurement.” 1991. QA :3
40. C. L. Wyatt, V. Privalsky, and R. Datla, Recommended practice; symbols, terms, units, and uncertainty analysis for radiometric sensor calibration, NIST Handbook 152 (1998)
41. T. C. Larason, S. S. Bruce, and A. C. Parr, “Spectroradiometric Detector Measurements.” NIST Special Publication, 250-41, 1998. QA :4

42. S. W. Brown, G. P. Eppeldauer, and K. R. Lykke, NIST Facility for spectral irradiance and radiance responsivity calibrations with uniform sources, *Metrologia* 37, 579–582 (2000).
43. G. P. Eppeldauer, et al., Realization of a spectral radiance responsivity scale with a laser-based source and Si radiance meters, *Metrologia* 37, 531–534 (2000).
44. V. E. Anderson, N. P. Fox, and D. H. Nettleton, Highly stable, monochromatic and tunable optical radiation source and its application to high accuracy spectrophotometry, *Appl. Opt.* 31, 536–545 (1992).
45. M. Noorma, et al., Characterization of filter radiometers with a wavelength-tunable laser source, *Metrologia* 40, S220–S223 (2003).
46. A. R. Schaefer and K. L. Eckerle, Spectrophotometric tests using a dye-laser-based radiometric characterization facility, *Appl. Opt.* 23, 250–256 (1984).
47. N. P. Fox, et al., High-accuracy characterization and applications of filter radiometers, *Proc. SPIE* 2815, 32–41 (1996).
48. A. Sperling, *personal communication*.
49. A. R. Schaefer, R. D. Saunders, and L. R. Hughey, Intercomparison between independent irradiance scales based on silicon photodiodes physics, gold-point blackbody radiation, and synchrotron radiation, *Opt. Eng.* 25, 892–896 (1986).
50. K. D. Mielenz, R. D. Saunders, and J. B. Shumaker, Spectroradiometric determination of the freezing temperature of gold, *J. Res. Natl. Inst. Stand. Technol.* 95, 49–67 (1990).
51. Spectralon, Labsphere, Inc., North Sutton, NH.
52. Infragold, Labsphere, Inc., North Sutton, NH.
53. J. Fowler and M. Litorja, Geometric area measurements of circular apertures for radiometry at NIST, *Metrologia* 40, S9–S12 (2003).
54. T. Larason, et al., Responsivity calibration methods for 365-nm irradiance meters, *IEEE Trans. Instrum. Meas.* 50, 474–477 (2001).
55. P.-S. Shaw, R. Gupta, and K. R. Lykke, Characterization of an ultraviolet and vacuum ultraviolet irradiance meter with synchrotron radiation, *Appl. Opt.* 41, 7173–7178 (2002).
56. C. A. Schrama and H. Rejin, Novel calibration method for filter radiometers, *Metrologia* 36, 179–182 (1999).
57. C. E. Gibson, B. K. Tsai, and A. C. Parr, “Radiance Temperature Calibrations.” NIST Special Publication, 250-43, 1998.
58. A. C. Parr, “A National Measurement System for Radiometry, Photometry, and Pyrometry Based upon Absolute Detectors.” NIST Technical Note 1421, 1996.
59. E. F. Zalewski and C. R. Duda, Silicon photodiode device with 100% external quantum efficiency, *Appl. Opt.* 22, 2867–2873 (1983).

60. T. J. Quinn and J. E. Martin, A radiometric determination of the Stefan-Boltzmann constant and thermodynamic temperatures between -408°C and $+1008^{\circ}\text{C}$, *Phil. Trans. Roy. Soc. London A* 316, 85 (1985).
61. J. E. Martin, N. P. Fox, and P. J. Key, A cryogenic radiometer of absolute radiometric measurements, *Metrologia* 21, 147 (1985).
62. C. L. Cromer, G. Eppeldauer, J. E. Hardis, T. C. Larason, and A. C. Parr, National Institute of Standards and Technology detector-based photometric scale, *Appl. Opt.* 32, 2936–2948 (1993).
63. Y. Ohno, “NIST Measurement Services: Photometric Calibrations.” NIST Special Publication 250-37, 1997
64. C. L. Cromer, G. Eppeldauer, J. E. Hardis, T. C. Larason, Y. Ohno, and A. C. Parr, The NIST detector-based luminous intensity scale, *J. Res. Natl. Inst. Stand. Technol.* 101–102, 109–131 (1996).
65. Y. Ohno, Improved photometric standards and calibration procedures at NIST, *J. Res. Natl. Inst. Stand. Technol.* 102, 323–331 (1997).
66. H. Preston-Thomas, The International Temperature Scale of 1990 (ITS-90), *Metrologia* 27, 3–10 (1990).
67. J. H. Walker, R. D. Saunders, and A. G. Hattenburg, “Spectral Radiance Calibrations.” Natl. Bur. Stand. Spec. Publ. 250-1, Washington: U.S. Government Printing Office, 1987.
68. A. R. Schaefer and R. D. Saunders, Intercomparison between silicon and blackbody radiometry using a silicon photodiode/filter radiometer, *Appl. Opt.* 23, 2224–2226 (1984).
69. R. D. Saunders, et al., Realization of new NIST radiation temperature scales for the 1000 K to 3000 K region using absolute radiometric techniques, *Temperature, Measurement and Control in Science and Industry* 323, 221–225 (1993).
70. H. W. Yoon, C. E. Gibson, and P. Y. Barnes, Realization of the National Institute of Standards and Technology detector-based spectral irradiance scale, *Appl. Opt.* 41, 5879–5890 (2002).
71. H. W. Yoon, et al., Temperature scales using radiation thermometers calibrated from absolute irradiance and radiance responsivity, in *NCSL International Workshop and Symposium*, Orlando, FL, 2003.
72. H. W. Yoon, et al., The realization and the dissemination of the detector-based kelvin, submitted to *Proc. Tempmeko 04*, Dubrovnik, Croatia, 2004.
73. H. W. Yoon and C. E. Gibson, A comparison of the absolute detector-based spectral radiance assignment with the current NIST assigned spectral radiance of tungsten-strip lamps, submitted to *Proc. Tempmeko 04*, Dubrovnik, Croatia, 2004.

74. G. Machin, et al., A comparison of ITS-90 and detector-based scales between NPL and NIST using metal-carbon eutectics, submitted to *Proc. Tempmeko 04*, Dubrovnik, Croatia, 2004.